JIANHAN WU

MASTER OF SCIENCE THESIS

CHARACTERIZATION OF ACLY KNOCKDOWN IN HEPATOCELLULAR CARCINOMA

By JIANHAN WU, B.HSc

A Thesis Submitted to the School of Graduate Studies in Partial Fulfillment of the Requirements for the Degree Master of Science

MASTER OF SCIENCE (2020) Department of Medical Sciences: Nutrition & Metabolism

McMaster University, Hamilton, Ontario, Canada

Title: Characterization of ACLY knockdown in hepatocellular carcinoma

Author: Jianhan Wu, B.HSc.

Supervisor: Dr. Gregory R. Steinberg, Ph.D.

Number of pages: 65

LAY ABSTRACT:

Cancer is a disease characterized by the uncontrolled proliferation of abnormal cells. However, this characteristic requires cancer cells to access sufficient supplies of nutrients. While traditionally glucose has been implicated as a driver of tumor growth, recent evidence has emerged implicating lipid as a key resource for various molecular functions related to cell proliferation. In this study, we traced lipid synthesis to its root, acetyl-CoA, and elucidated the consequences of suppressing the enzyme responsible for synthesizing acetyl-CoA, ATP citrate lyase (ACLY), in human liver cancer cells. We found that by reducing the quantity of ACLY in cells, various parameters of lipid metabolism related to lipid synthesis and breakdown were altered. In parallel, we also found that this negatively affected various measures of cell proliferation and tumor growth. Collectively, findings of this study suggest that therapeutic targeting of ACLY may be a promising avenue of research for the treatment of liver cancer.

ABSTRACT:

Lipid is co-opted by cancer cells to meet the metabolic demands of uncontrolled cell proliferation. ATP citrate lyase (ACLY) plays an important role in lipid metabolism by catalyzing the synthesis of acetyl-CoA from mitochondrial citrate thus providing the essential cytosolic precursor for subsequent fatty acid/cholesterol synthesis. Previously, we demonstrated that inhibition of acetyl-CoA carboxylase (ACC) leads to impaired hepatic DNL and reduced incidence of hepatocellular carcinoma (HCC). Given that ACC acts downstream of ACLY, herein, we characterized the role of ACLY as a lipid metabolic regulator of HCC progression. Sourcing from publicly available patient transcriptome datasets, we found that ACLY expression positively correlates with HCC progression and mortality. Inducible knockdown of ACLY expression in Hep3B and SK-Hep1 cells reprograms lipid metabolism through reducing glucose mediated de novo lipogenesis (DNL), inducing fatty acid oxidation and upregulating acetate mediated DNL via the acyl-CoA synthetase 2 (ACSS2) pathway. This is accompanied by decreased cell proliferation, colony formation and invasion. In vivo, orthotopic modeling of human HCC in immune-compromised NOD-*Rag1*^{null} *IL2rg*^{null} (NRG) mice using Hep3B cells results in reduced tumor weight upon ACLY knockdown.

ACKNOWLEDGMENTS:

Throughout the duration of my research-based thesis, I have had the support of many individuals without whom this work would have not been possible. Firstly, I would like to thank Dr. Gregory R. Steinberg for providing me with the resources and guidance necessary for me to grow as a scientist and for being a role model, demonstrating the importance of collaboration and big-picture thinking in scientific research. I would also like to thank our collaborators Dr. Theodoros Tsakiridis, Dr. Paola Muti and Dr. Jonathan Bramson for providing valuable insights and resources, enabling the completion of this project.

The day-to-day work involved in research works best with a great laboratory environment, and for that I would like to thank everyone in the Steinberg and Tsakiridis lab for being wonderful people to work with. Among those who I worked closely with, I would like to thank Dr. James S. Lally and Dr. Jaya Gautam for being the most understanding, accommodating and patient mentors that I have had the pleasure to learn from. To all my fellow peers and seniors in the lab, I would like to thank each and every one of you for your kind assistance and friendship through the past two years and the memories that I shall cherish for life. Furthermore, to my undergraduate mentors and peers in Dr. Gurmit Singh and Dr. John A. Hassell's laboratories, thank you for opening my mind to the world of cancer research and for laying the foundational skillsets upon which many components of this thesis work draw from.

Lastly, I would like to thank my parents for their unconditional love and support. I would also like to thank my significant other, Eulaine, for being there through thick and thin with me. And to all my wonderful families, friends, and mentors since my adolescent years, thank you for shaping me into the person I am today.

Table of Contents

LIST OF FIGURES AND TABLES

LIST OF ABBREVIATIONS

ACC - acetyl-CoA carboxylase

ACLY – ATP citrate lyase

ACSS2 - acyl-coenzyme A synthetase short-chain family member 2

AKT – protein kinase B

AMPK – 5'-adenosine monophosphate activated protein kinase

ATP – adenosine triphosphate

CPT – carnitine palmitoyltransferase

DEN – diethylnitrosamine

DNL – de novo lipogenesis

FAO – fatty acid oxidation

FASN – fatty acid synthase

HCC – Hepatocellular Carcinoma

HBV/HCV – hepatitis B/C virus

NASH – non-alcoholic steatohepatitis

SCD1 – stearoyl-coenzyme A desaturase-1

shRNA – short hairpin RNA

SREBP – sterol regulatory element-binding protein

T2D – type 2 diabetes

TCA – citric acid cycle

CHAPTER I – INTRODUCTION

1.1 Hepatocellular Carcinoma

1.1.1 Overview and Treatment

Globally, HCC is the third most common cause of death from cancer and its incidence is on the rise.[1] In Canada, the incidence of HCC is the second leading cancer among both males and females as determined by average annual percentage change from 1985 – 2015.[2] However, treatment options for HCC are limited for approximately 85% of patients who are unsuitable for surgical resection or liver transplantation, the gold standard treatments for early HCC.[3] Unfortunately, most patients are not diagnosed at the early stage of the disease. Furthermore, those who undergo curative treatments often experience metastatic recurrence within two years after surgery and at a rate of 70% over five years.[4,5] While other non-surgical therapies exist, such as radio- and chemoembolization, the caveat remains that these therapies are unable to produce favorable outcomes in patients with advanced disease.[3] Currently, Sorafenib and Lenvatinib are the only two first line pharmacotherapies for advanced HCC. Yet, they could only extend median survival and time to progression by approximately 3 – 4 months, a far cry compared to the effects of similar targeted therapies for other common cancer types.[6,7] As such, development of novel therapies for advanced HCC are needed.

1.1.2 Etiology

Predominantly, HCC is characterized by chronic liver injury and inflammation. Traditionally, these damages are thought to be derived from HBV/HCV infections and excessive exposure to xenobiotics.[8] However, in recent years, metabolic syndromes such as NASH and T2D have also emerged as risk factors for HCC.[9,10] These metabolic syndromes lead to the intrahepatic accumulation of lipids which cause mitochondrial dysfunction and endoplasmic reticulum stress. Due to the regenerative capacity of the liver, injuries to the liver parenchyma are promptly rescued by proliferation of hepatocytes and activation of hepatic stellate cells.[8] However, with each recurrence of injury and regeneration, scar tissues are generated from matrix producing stellate cells and their differentiation towards a myofibroblast phenotype, leading to the formation of fibrosis and eventually cirrhosis. While these metabolic and structural aberrations may seem unrelated to tumorigenesis, a process deeply rooted in genetic mutations, they indirectly cause tumor transformation through exposing cells to excessive oxidative stress, chronic inflammation, growth factors and cytokines. Hepatocytes under these stressors are more prone to acquire genetic mutations and epigenetic alterations capable of initiating tumor transformation, leading to the onset of HCC.[11] Currently, limited data is available for determining driver mutations contributing towards HCC. This may be due to the heterogeneous clinical features and etiologies associated with HCC. However, specific genetic mutations enriched in some HCC subtypes have been identified, though none are characteristically defining. For example, aberrant activating mutations of telomerase reverse transcriptase are the most common genetic mutations in HCC and are enriched in HCC related to alcohol

consumption. Additionally, inactivating mutations of tumor protein 53 are enriched in HCC related to HBV infection.[11] To our knowledge, no mutation enrichment has been identified in association with NASH related HCC. Collectively, the lack of targetable somatic mutations present in HCC may indicate a need to look beyond genetic mutations for therapeutic targets. This notion is supported by a novel classification of HCC based on metabolic characteristics which revealed distinct subtypes of HCC with differential prognosis as well as subtype specific enzymes that could potentially be modulated to control HCC progression.[12] As such, for NASH related HCC, perhaps reprogramming lipid metabolism could be of significant therapeutic interest.

1.2 Lipid Metabolism

1.2.1 De Novo Lipogenesis

While carbohydrate metabolism has historically been the focus of cancer metabolism research, in recent years, lipids have gained traction due to their encompassing roles across a spectrum of molecular functions featuring membrane synthesis, second messenger signaling and energy storage, all of which are essential for increased cell proliferation. Unlike most healthy human tissues which preferentially utilize exogenous lipid from dietary sources, cancer cells preferentially utilize endogenous lipid synthesis to meet their elevated metabolic demands.[13] This is true for HCC where genes involved in DNL are ubiquitously upregulated while fatty acid uptake is reduced in tumor compared to healthy adjacent liver tissue.[14] Transcriptionally, the regulation of DNL pathway is primarily controlled by sterol regulatory element-binding proteins (SREBPs).[15] Biochemically, the

process begins with the conversion of glucose, acetate or fatty acid derived mitochondrial acetyl-CoA into citrate via the TCA cycle.[16] Subsequently citrate is exported into the cytosol where it is converted into cytosolic acetyl-CoA by ACLY or ACSS2. The fate of cytosolic acetyl-CoA is varied, however in the context of DNL, it is carboxylated by ACC into malonyl-CoA which is then converted to palmitate or other types of fatty acids by FASN. Finally, fatty acids are converted to monounsaturated fatty acids by SCD1 which are then able to contribute towards various cellular functions such as signal transduction and membrane synthesis via conversion to diacylglycerol, energy storage via conversion to triacylglycerol and ATP production through the process of FAO.

1.2.2 Role of DNL in HCC

Functionally, various components of the DNL pathway have been shown to play an important role in HCC onset and progression. Lally et al. recently demonstrated elevated DNL and increased incidence of tumor lesions in a rat model of HCC through inactivating point mutation of the inhibitory phosphorylation sites on both isoforms of ACC.[17] ACC is involved in the conversion of acetyl-CoA to malonyl-CoA, the first committed substrate for lipogenesis. Inhibition of ACC1/2 using a hepato-selective chemical inhibitor reduced HCC lesions and prolonged survival in a pre-clinical setting. Consistent with this, genetic silencing of FASN, the subsequent step in DNL, also prevented HCC onset in an AKT overexpressing mouse model through inhibition of the AKT/mammalian target of rapamycin complex 2 pathway.[18] Interestingly, DNL also plays a role in tumor stemness. Inhibition of SCD1 suppressed sphere forming capacity and tumor-initiating cell related

gene expression in Huh7 and Hep3B HCC cell lines.[19] This was further corroborated by a patient derived sorafenib-resistant xenograft HCC model which showed that inhibition of SCD1 induced tumor differentiation and re-sensitized tumor cells to sorafenib treatment.[20] Collectively, these findings demonstrate significant therapeutic potential underlying DNL inhibition for the treatment of HCC. This is further reinforced by a metabolic network-based stratification of HCC patients which showed that elevated DNL, glycolysis and reduced FAO are among the defining characteristics of the HCC subtype associated with the most malignant outcome.[12]

1.2.3 Role of Fatty Acid Oxidation in HCC

FAO begins with the translocation of fatty acyl-CoA molecules into the mitochondria via CPT1 and CPT2.[16] Once inside the mitochondrial matrix, a series of reactions shorten fatty acid carbon chains by two carbons each cycle to produce NADH, $FADH_2$ and acetyl-CoA. These molecules then contribute to the citric acid cycle which ultimately yields ATP.

Recent studies have shown that FAO derived ATP is essential for solid tumor cells escaping anoikis caused by loss of extracellular matrix attachment and the resultant deprivation of glucose.[21] Similarly, FAO has been shown to perform a protective and supportive role in HCC under conditions of nutrient starvation and anti-angiogenic treatment induced hypoxia in steatotic livers.[22,23] This effect is fine tuned by AMPK which relieves FAO suppression by the lipogenic enzyme ACC and its substrate malonyl-CoA upon sensing energy stress.[23,24]

However, the effect of FAO is not definitive and may be highly variable between HCC subtypes. In fact, hypoxia downregulates the expression of FAO related genes in tumors transplanted in non-steatotic livers.[23] This parallels in vitro data in Hep3B and HepG2 cells which demonstrate impaired expression of medium- and long-chain acyl-CoA dehydrogenases and FAO under hypoxic conditions via regulation by hypoxia inducible factor 1α.[25] The inhibition of FAO enhances Hep3B xenograft growth through reduced reactive oxygen species levels and suppression of phosphatase and tensin homolog expression as a result of monounsaturated fatty acid accumulation. The effect of FAO inhibition in promoting tumor growth is further supported by the role of CD147 in HCC. CD147 can simultaneously stimulate DNL while suppressing FAO and its genetic ablation led to reduced tumor proliferation and metastasis in a mouse orthotopic model.[26] In line with this, acylcarnitine species also accumulated as a result of CPT2 downregulation in both human NASH-HCC tissues and in various mouse models of HCC exhibiting hepatosteatosis.[27] This led to enhanced hepatocarcinogenesis and tolerance of lipotoxicity via signal transducer and activator of transcription 3 activation and c-Jun N-terminal kinase attenuation respectively. These findings suggest impaired FAO may be an unfavorable prognostic marker for HCC. Indeed, stratification of HCC patients based on metabolic activity indicate that the HCC subtype with the most favorable survival outcome exhibit the highest FAO activity while the least favorable outcome is associated with the lowest FAO but the highest DNL activity.[12] However, whether or not FAO plays a driver or a passenger role in the progression of HCC remains open to investigation.

1.2.4 Role of Cholesterol in HCC

Cholesterol is involved in various cellular functions such as maintaining cellular membrane integrity, intracellular transport, and cell signalling. Like the process of DNL, cholesterol synthesis uses the same cytosolic acetyl-CoA precursor and is controlled transcriptionally by SREBPs.[15] Intracellular cholesterol originates from either endogenous synthesis via the mevalonate pathway or serum cholesterol uptake via low-density lipoprotein receptor. While serum cholesterol is a key player in metabolic diseases, studies have provided conflicting reports with respect to its role in tumor progression. Epidemiological studies have suggested that serum cholesterol lowering is associated with increased incidence of cancer.[28,29] In the context of HCC, a retrospective analysis of 1141 HCC patients identified an inverse correlation between serum cholesterol levels and both disease free and overall survival.[30] This was corroborated by another retrospective case-control analysis of 969 HCC patients which identified high serum cholesterol level as an independent predictor of improved overall survival.[31] A preclinical study shows that supplementation of a high cholesterol diet in immune-compromised mice decreased the incidence of intravenous lung metastasis and spleen to liver metastasis as a result of increased sequestration of CD44 to lipid rafts, preventing its interaction with pro-metastatic effector substrates.[31]

On the other hand, proteomic profiling of early HBV induced HCC tumor and paired non-tumor samples identified that protein signatures associated with disrupted cholesterol metabolism characterized the HCC subtype with the most malignant clinical outcome.[32] In vitro, genetic knockdown of sterol-O-acyltransferase 1 inhibited cholesterol localization to

the cell membrane and disrupted the expression of several membrane bound receptors important for tumor proliferation and metastasis. Furthermore, dietary cholesterol intake was found to accelerate hepatocarcinogenesis in mice injected with diethylnitrosamine (DEN) and fed with a high-fat diet.[33] Interestingly, mice receiving cholesterol supplemented high-fat diet also developed NASH prior to HCC compared to mice receiving high-fat diet alone, demonstrating the experimental model's biological relevance to human HCC. This was corroborated by similarities in transcriptional alterations identified in human NASH-HCC tumor vs. non-tumor samples.

The divergent findings concerning the roles of cholesterol in HCC described in these studies highlight the complexity of the subject and the context dependence thereof. Tumor metastasis occurs through an intricate migration and invasion cascade in contrast to the onset of primary tumor.[34] As such, experimental findings on HCC metastasis may vary based on whether or not tumor cells were injected intravenously or orthotopically. Furthermore, DEN injection results in spontaneous onset of HCC through inducing DNA mutation, oxidative stress and inflammation.[35] Cholesterol supplementation may synergize with these effects in an auxiliary role to accelerate the onset of primary HCC. As such, findings using the DEN model may be absent in tumor graft models that are lacking in microenvironment reprogramming. Therefore, research findings with respect to cholesterol supplementation may be variable depending on the experimental model.

1.3 Role of ACLY in Cancer

ACLY is the first step of DNL and its expression and activity are upregulated in various types of cancer such as lung, colon, breast and prostate cancer.[36,37,38] By catalyzing the synthesis of acetyl-CoA from mitochondrial citrate, ACLY provides the essential cytosolic precursor for subsequent lipid metabolic processes (Figure 1).[39] Furthermore, acetyl-CoA is involved in protein and histone acetylation which directly regulates cell signaling pathways and gene expression. The dual role of ACLY enables the unique coordination of metabolic adaptation in response to changing nutrient availability which is important for sustaining the rapid proliferation and growth of tumor.

Several reports have already shown the anti-tumor effects of ACLY inhibition in various types of cancer both in vitro and in vivo.[36,40,41] However, a dedicated study on the effect of ACLY inhibition in HCC does not exist. Interestingly, the anti-tumor effects of ACLY inhibition seem to be cell line dependent. Specifically, cancer cells exhibiting more glycolytic phenotype are more sensitive to ACLY inhibition.[40] This is in line with the role of ACLY linking carbohydrate and lipid metabolism. Since glycolytic tumors are often associated with poor clinical outcome, the effects of ACLY inhibition may also be most pronounced in advanced grade tumors.[42]

1.3.1 ACLY Involvement in Lipid Metabolism and Metabolic Diseases

Cytosolic acetyl-CoA contributes toward various metabolic processes beyond DNL. Hence, modulation of its activity may result in cascading effects with respect to lipid metabolism. ACLY indirectly plays a role in FAO via regulation of malonyl-CoA availability. Malonyl-CoA inhibits CPT1 mediated mitochondrial FAO by acting as a

competitive inhibitor against fatty acid substrates.[43] Acetyl-CoA is converted to malonyl-CoA via ACC. Therefore, inhibition of ACLY may relieve the suppressive effects of malonyl-CoA on FAO. Furthermore, ACLY also plays a role in cholesterol synthesis via the mevalonate pathway. Specifically, cytosolic acetyl-CoA is converted to acetoacetyl-CoA which is then catalyzed by 3-hydroxy-3-methyl-glutaryl-coenzyme A synthase for cholesterol synthesis.[16] As such, inhibition of ACLY may suppress cholesterol synthesis in addition to DNL.

Unsurprisingly, the multi-faceted roles of ACLY in lipid metabolism have implicated ACLY in the etiology of various metabolic diseases. Particularly, a large cohort mendelian randomization study identified genetic variants of ACLY leading to differential plasma LDL cholesterol lowering phenotypes corresponding to varying levels of cardiovascular disease risks.[44] With respect to the liver, it was found that liver specific depletion of ACLY via adenovirus RNA interference prevented leptin receptor deficient mice from developing hepatic steatosis and transcriptionally impaired lipogenic gene expression.[45] Since metabolic syndromes are risk factors for developing NASH and HCC, these findings prompt further investigation of the role of ACLY in HCC.

1.3.2 Involvement of AKT and Epithelial-to-Mesenchymal Transition (EMT)

ACLY inhibition has been reported to suppress tumor stemness and induce tumor differentiation.[36,40,41] This has been observed as a consequence of AKT inhibition.[41] Traditionally, AKT is thought to act upstream of ACLY via activating phosphorylation of Ser454.[46] However, a study in A549 and H1650 lung cancer cells showed remarkably

reduced AKT phosphorylation and activation upon ACLY knockdown. In turn, this resulted in the upregulation of E-cadherin expression and downregulation of Vimentin expression, both structural proteins, as well as reduction in the expression of the transcription factor Snail.[47] E-cadherin, Vimentin and Snail are downstream targets of the PI3K-AKT pathway and are key components of (EMT) process for which advanced grade, metastatic, treatment resistant and tumour-initiating cancer cells are known to undergo.[48] Therefore, it is unsurprising that several studies have reported a role for ACLY inhibition in the differentiation of poorly differentiated lung cancer, breast cancer and leukemia cell cells.[40,49,50,51] Hence, it is possible that similar effects may be observed in the context of HCC, where ACLY inhibition is capable of reducing AKT phosphorylation and activation along with suppressing EMT.

1.3.3 Compensatory Sources of Acetyl-CoA

Citrate catalyzed by ACLY is not the only synthetic source of intracellular acetyl-CoA. ACSS2 is a cytosolic enzyme that catalyzes the synthesis of acetyl-CoA using acetate derived from extracellular sources or intracellular deacetylation processes.[52] ACSS2 can compensate for acetyl-CoA synthesis in the absence of ACLY.[52] Furthermore, inhibition of ACSS2 has shown to reduce hepatic tumor burden in a genetically induced spontaneous HCC mouse model.[53] The existence of a compensatory and redundant mechanism may rescue the effect of ACLY inhibition in HCC. A recent study found that fructose overfeeding in mice increases liver triglyceride independently of liver ACLY due to fructose conversion to acetate by the gut microbiome.[54] However, whether this is important

under physiological conditions in humans remains to be determined. For example, other studies have shown that physiological levels of fructose are largely metabolized into glucose by the gastrointestinal tract while the inhibition of ketohexokinase, the primary enzyme metabolizing fructose, reduces hepatic lipid accumulation.[55] Nevertheless, the involvement of acetate is important to consider when characterizing the role of ACLY in HCC.

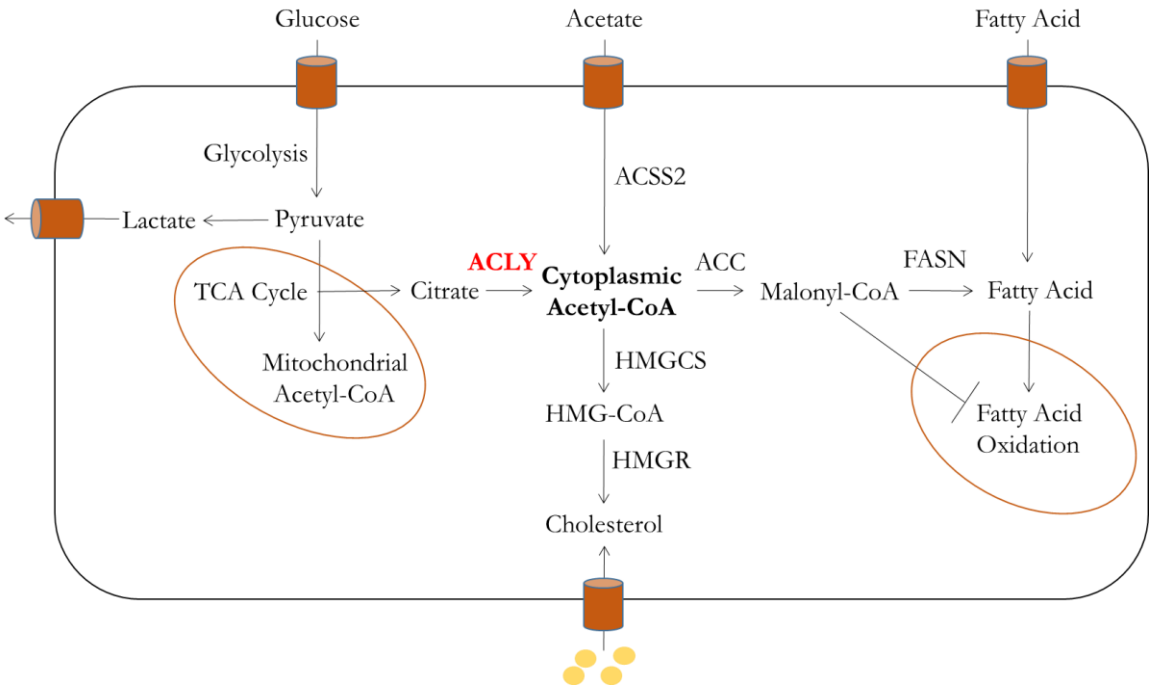

Figure 1 – Role of ACLY in lipid metabolism. ACLY catalyzes the synthesis of cytoplasmic acetyl-CoA using mitochondrial derived citrate from glucose. ACSS2 is an alternative source of acetyl-CoA synthesis by utilizing acetate derived from extracellular environment or intracellular deacetylation processes. Acetyl-CoA is an important substrate for lipid metabolism and may be implicated in the progression of liver disease towards HCC.

1.4 Objectives and Hypothesis

We hypothesized that ACLY genetic inhibition could reprogram lipid metabolism leading to anti-tumor effects. Our first objective was to elucidate the role of ACLY expression in HCC disease progression and patient survival using publicly available transcriptome datasets. We then aimed to engineer doxycycline (DOX) inducible short hairpin RNA (shRNA) constructs to suppress ACLY expression in human HCC cell lines for the purpose of phenotypic characterizations. Specifically, this involved in vitro analysis of targeted protein expression, characterization of cell proliferation, clonogenicity and migration, as well as radiolabelled substrate tracing of DNL, sterol synthesis and FAO processes. Lastly, we characterized ACLY deficient tumor growth through orthotopic injection of engineered Hep3B cells in an immune-compromised mouse model.

CHAPTER II – METHODS AND MATERIALS

Chapter II – Methods and Materials

2.1 Cell Culture

Hep3B (ATCC HB-8064) and SK-Hep1 (ATCC HTB-52) were cultured adherently using Eagle's Minimum Essential Medium (EMEM) (ATCC 30-2003) supplemented with 10% (v/v) fetal bovine serum (FBS) (Gibco Cat. No.10437-028) and 1% (v/v) antibiotic-antimycotic solution (Gibco Cat. No. 15240112). HEK293T (ATCC CRL-3216) was cultured adherently using Dulbecco's Modified Eagle Medium (DMEM), high Glucose (Gibco Cat. No. 11965092) supplemented with 10% (v/v) FBS and 1% (v/v) antibiotic-antimycotic solution as aforementioned along with 1% (v/v) L-Glutamine (Gibco Cat. No. 25030081), 1% (v/v) MEM Non-Essential Amino Acids Solution (Gibco Cat. No. 11140050) and 1% (v/v) Sodium Pyruvate (Gibco Cat. No. 11360070).

Cells were grown in tissue culture flasks. Upon reaching 80-90% confluency, cells were trypsinized using Trypsin-EDTA (0.25%), phenol-red (Gibco Cat. No. 25200072). Cell suspensions were then centrifuged at 500 x g for 5 minutes at room temperature. Resulting pellet was quantified, resuspended in standard media, re-seeded into a second tissue culture flask at a ratio of 1:10 (v/v) and incubated at 37°C, 5% CO_2.

2.2 Cell Proliferation and Viability Assay

Prior to passaging, cells were seeded in 96 well plates at a concentration of 25,000 cells/mL in volumes of 200 µL and incubated at 37°C, 5% CO_2 overnight. Chemicals were

applied to each well as necessary at a final concentration that does not exceed 1% of total solution volume. Chemical treatments were applied for a total duration as determined by individual experiments. If exceeding 48 hours, new treatments were applied using fresh media in a manner consistent with initial treatment. For quantification of cell viability, PrestoBlue Cell Viability Reagent (Invitrogen Cat. No. A13261) was added to 10% of the solvent volume and incubated for one hour prior to fluorescence detection using SpectraMax M5 (Molecular Devices).

2.3 Colony Formation Assay

Cells were seeded into 12 well plates at a density of 500 cells per well and incubated at 37°C, 5% CO_2. Media replenishment and chemical treatment occurred every 2-3 days and colony formation were followed for 7 days. After the incubation period, the media was removed, and cells were washed with PBS (Gibco Cat. No. 10010023) and fixed with 100 µL of 10% formalin for 30 minutes at room temperature. Subsequently, 500 µL of 0.5% crystal violet DNA stain (Sigma-Aldrich Cat. No. 0775) was applied for 10 minutes at room temperature. At the conclusion of staining, crystal violet solution was rinsed from the plates and plates were washed with water to remove residual stain. Plates were then dried at room temperature overnight. Viable colonies (≥ 50 cells) were counted under light microscopy at 100x magnification.

2.4 Generation of Stable Cell Lines

2.4.1 Plasmid Construction

DOX inducible shACLY plasmid vectors were generated using the inducible EZ-Tet-pLKO-Hygro vector (Addgene Plasmid No. 85972).[56] Two ACLY shRNA sequences (1) 5' CGTGAGAGCAATTCGAGATTA 2) 5' GGCATGTCCAAGCTCAA) and one non-targeting shRNA sequence (5' CCTAAGGTTAAGTCGCCCTCG) were ligated, transformed, amplified and validated using established protocol as described.[56]

2.4.2 Lentivirus Production

2nd generation lentivirus production system was used to generate high-titer lentivirus. HEK293T cells were incubated with psPAX2 (Addgene Plasmid No. 12260), pMD2.g (Addgene Plasmid No. 12259) and the EZ-Tet-pLKO-Hygro (Addgene Plasmid No. 85972) transfer plasmid at a ratio of 1:1:2 pmol in the presence of Lipofectamine 2000 in Opti-MEM. 16 hours post transfection, media was changed to 1% bovine serum albumin (Sigma Aldrich Cat. No. A1470) and 1 mM Na-Butyrate (Tocris Cat. No. 3850) supplemented antibiotic free DMEM (Gibco Cat. No. 11965092) for HEK293T cell culture as described in 2.1. 48 hours post transfection, lentivirus media was collected and mixed with Lenti-X concentrator (Takara Cat. No. 631232) prior to storing overnight at 4°C. Next day, lentivirus was concentrated through centrifugation at 1,500g for 45 minutes at 4°C. Resulting pellet was resuspended at 1:10 of initial media volume, aliquoted and frozen in liquid nitrogen for storage.

2.4.3 Lentivirus Transduction

An initial dilution of 1:50 v/v followed by serial dilutions of 1:4 v/v were used to transduce target cell lines at 60,000 cells per well in 6 well plates using 5 µg/mL polybrene (Sigma Aldrich Cat. No. 107689) supplemented cell culture media as described in 2.1. Cells were transduced for 24 hours, followed by recovery in lentivirus free media for another 24 hours prior to selection of successfully transduced cells using a pre-determined, cell line dependent concentration of Hygromycin B (Sigma Aldrich Cat. No. H3274) or Puromycin (Sigma Aldrich Cat. No. P8833) for 7 days.

2.4.4 Cell Line Generation

Polyclonal populations arose from cells that survived antibiotic selection. Upon reaching 80-90% confluence in 6 well plates, they were serially passaged in T25 and T75 cell culture flasks. After the initial passage in T75 flasks, cells were frozen in 1mL, 1×10^6 cells/mL aliquots in 10% dimethyl sulfoxide (DMSO) (Sigma Aldrich Cat. No. D4540) supplemented cell culture media as described in 2.1.

2.5 Immunoblot

2.5.1 Protein Lysate Harvest, Quantification and Preparation

Cells were washed with cold PBS (Gibco Cat. No. 10010023) and scraped with 100 – 200 µL of cold cell lysis buffer (50 mM HEPES pH 7.4, 150 mM NaCl, 100 mM NaF, 10 Na-pyrophosphate, 5 EDTA mM , 250 mM sucrose, 1 mM DTT, and 1 mM Na-orthovanadate, 1% Triton X, and Complete Protease Inhibitor Cocktail (Roche Cat. No.

11836153001)). Solution samples were collected and centrifuged at 13,000g for 10 minutes at 4°C to isolate protein fraction from cell debris.

For tissue samples, frozen tissues were cut into pieces < 30 mg and aliquoted in cryotubes containing cold cell lysis buffer and 2 ceramic beads. Samples were placed in Precellys 24 Homogenizer (Bertin Technologies Cat. No. 10144-622) and homogenized at 5,500 rpm for two 30 seconds cycles prior to end-over-end rotation for 30 minutes at 4 °C. Solution samples were collected and centrifuged at 13,000g for 10 minutes at 4°C to isolate protein fraction from cell debris.

Protein samples were quantified for peptide concentration using the Pierce BCA Protein Assay Kit (Thermo Scientific Cat. No.23225) according to instruction. Samples were then diluted to 1 µg/µL using 4X SDS sample buffer (40% glycerol, 240 mM, Tris-HCl pH 6.8, 8% SDS, 0.04% bromophenol blue, 5% β-mercaptoethanol, 20 mM DTT) and cell lysis buffer. Samples were then boiled for 5 minutes at 95 °C prior to immunoblotting.

2.5.2 SDS-PAGE, Transfer and Blocking

SDS polyacrylamide gels were prepared at 10% or 12% polyacrylamide concentration dependent on protein size. 25 µg of protein sample was loaded into each lane. Gel electrophoresis was performed first at 90V as protein travels through the stacking gel and then 120V, through the separating gel. Protein samples were then transferred onto a PVDF membrane (Roche Cat. No. 03010040001) at 4°C for 90 minutes following the standard wet transfer protocol. Subsequently, membranes were rinsed and rocked gently with 1X TBS (50 mM Tris, 150 mM NaCl, 1 M HCl, pH 7.4) for 3 cycles of 5 minutes each

then blocked using a TBST-BSA solution (1X TBS, 0.5% bovine serum albumin, 0.1% tween-20) for 1 hour at room temperature.

2.5.3 Immunodetection

Primary antibodies (Cell Signaling Technology) (Table 1) were diluted at 1:1000 in TBST-BSA solution. Membranes were then cut according to protein sizes and incubated in respective antibody solutions overnight at 4˚C with gentle rocking. Next day, primary antibody solutions were removed, and membranes were washed using TBST. Subsequently, membranes were incubated at room temperature with gentle rocking for 1 hour in solutions containing 1:10,000 dilution of species-specific secondary antibody (Cell Signaling Technology) conjugated to horseradish peroxidase. At the conclusion of incubation, membranes were washed again in TBST solution and kept in TBS solution until imaging and for storage.

Table 1 – Primary and secondary antibodies for immunoblotting

	Antibody	**Species**	**Dilution**
Primary	ACLY (Cat. No. 13390)	Rabbit	1:1000
	p-ACLY S455 (Cat. No. 4331)		1:1000
	ACSS2 (Cat. No. 3658)		1:1000
	FASN (Cat. No. 3180)		1:1000
	AKT (Cat. No. 4685)		1:1000
	p-AKT T308 (Cat. No. 13038)		1:1000
	p-AKT S473 (Cat. No. 4060)		1:1000
	β-actin HRP Conjugate (Cat. No. 12620)		1:5000
Secondary	Anti-rabbit IgG HRP-linked (Cat. No. 7074)	Goat	1:10000

2.6 DNL Assay

Cells were incubated in media supplemented with 1μCi [^{14}C] glucose (Perkin Elmer Cat. No. NEC042V250UC) and [^{3}H] acetate (Perkin Elmer Cat. No. NET003005MC) for 4 hours. Subsequently, cells were washed and scraped in PBS (Gibco Cat. No. 10010023). Lipids were extracted using a chloroform: methanol (1:2) solution, vortexed for 30 seconds and centrifuged at 13,000g for 10 minutes to isolate cellular debris and protein fractions from lipid supernatant. Lipids were further purified with chloroform: water (1:1) solution via vortex and centrifugation as described. Peptide concentration was quantified using the Pierce BCA Protein Assay Kit (Thermo Scientific Cat. No.23225) for normalization calculation. 100 μL of lipid supernatant was extracted from the non-polar chloroform phase and mixed with 5 mL of Ultima Gold Scintillation Fluid (Perkin Elmer Cat. No. 6013329) for radioactivity quantification.

2.7 Sterol Synthesis Assay

Cells were incubated in media supplemented with 1μCi [^{14}C] glucose (Perkin Elmer Cat. No. NEC042V250UC) and [^{3}H] acetate (Perkin Elmer Cat. No. NET003005MC) for 4 hours. Cells were washed with PBS (Gibco Cat. No. 10010023) and scraped in 0.5M KOH/EtOH solution. Samples were vortexed and heated for 2 hours at 70°C. Upon cooling to room temperature, 1 mL of water and 2 mL of n-hexane (Sigma Aldrich Cat. No. HX0293) were added and samples were vortexed for 30 seconds and centrifuged at 500g for 5 minutes at room temperature. Sterol fractions were obtained from the top phase of the

solution and mixed with 5 mL of Ultima Gold Scintillation Fluid (Perkin Elmer Cat. No. 6013329) for radioactivity quantification.

2.8 Fatty Acid Oxidation Assay

Cells were incubated with serum free cell culture media as described in 2.1 and supplemented with 2% bovine serum albumin (Sigma Aldrich Cat. No. A1470), 500 µM sodium palmitate (Sigma Aldrich Cat. No. P9787), 0.5µCi/mL [^{14}C] palmitic acid (Perkin Elmer Cat. No. NEC075H050UC) and 1 mM L-carnitine (Roche Cat. No. 11242008001) for 4 hours. Cell culture supernatant was collected at the end of incubation and mixed with 1 mL of 1M acetic acid (Fluka Cat. No. 34256-1L-R). Solution was sealed in a glass vial and shaken at 75 rpm, room temperature for 2 hours. Released CO_2 is absorbed in 450 µL of 1M benzethonium hydroxide (Sigma Aldrich Cat. No. B2156) during this time. Subsequently, tube containing benzethonium hydroxide is mixed with 5 mL of Ultima Gold Scintillation Fluid (Perkin Elmer Cat. No. 6013329) for radioactivity quantification.

2.9 Extracellular L-Lactate Assay

Cells were seeded at 200,000 cells/well in 6 well plates. After incubation for two days at 37°C, 5% CO_2, cell culture was replaced with serum free media and incubated for 4, 6 and 12 hours or treated with 200 µM phenformin (Sigma Aldrich Cat. No. P7045) for 6 hours. Cell supernatant was collected, centrifuged at 500g for 5 minutes and 2 µL of supernatant was directly used in L-Lactate assay (Cayman Chemical Cat. No. 700510)

according to protocol. Colorimetric intensity was measured using SpectraMax M5 (Molecular Devices).

2.10 Animal Experiment

All experiments were approved by the McMaster University Animal Ethics Committee and conducted under the Canadian guidelines for animal research (AUP 16-12-41).

2.10.1 Intrahepatic Tumor Injection

One day prior to surgery, male NOD-*Rag1*^{null} *IL2rg*^{null} (NRG) (mice kindly provided by the Bramson Laboratory) received intraperitoneal injections of 100 mg/kg cyclophosphamide and subcutaneous injections of 5 mg/kg carprofen.

1 hour prior to surgery, tumor cells were resuspended on ice in a 1:1 dilution of phenol red free Matrigel (Corning Cat. No. 356237) and cold PBS (Gibco Cat. No. 10010023), aliquoted in 50 µL volumes at a cell density of 2×10^7 cells/mL. During surgery, mice were anesthetized with 2% isoflurane (Baxter Cat. No. 1001936040), hair removed with 3-in-1 hair removal lotion (Nair Cat. No. 061700222611), and placed in supine position on a heating pad, with nose fitted in an anesthesia nose cone. The abdomen was disinfected and an approximately 2 cm horizontal incision was made below the left coastal margin from the midline of the abdomen. Separating the skin from the peritoneum, a second and smaller horizontal incision was made across the peritoneum to expose the liver. Next, the left lobe of the liver was withdrawn, stabilized, and tumor cells were injected into the liver

parenchyma while applying pressure using a cotton tipped applicator (Dynarex Cat. No. 4305) to enable hemostasis. Following injection, liver was returned into the peritoneal cavity and the peritoneum was closed with multiple single interrupted sutures using 4-0 Vicryl sutures (Ethicon Cat. No. J743D). The skin was closed using 9mm wound clips (Roboz Cat. No. RS-9262). Lastly, mice received post-surgical subcutaneous injections of 5 mg/kg carprofen, were placed in cages on a heating pad containing diet recovery gel (Clear H_2O Cat. No. 72-06-5022) and monitored until they were ambulatory.

2.10.2 Orthotopic Tumor Progression Experimental Design

Mice were monitored for recovery over the course of 7 days after surgery. Wound clips were removed on day 6 and mice were imaged for tumor progression on day 7 and weekly thereafter. Induction of *in vivo* shRNA expression was achieved via supplementing drinking water with 2 mg/mL DOX (Sigma Aldrich Cat. No. D9891) and 5% sucrose starting on day 7 post-surgery and every 2-3 days thereafter. In parallel, control mice were fed with drinking water supplemented with 5% sucrose without DOX. Tumor progression was followed until endpoint which is defined as the loss of >20% bodyweight. Mice were culled collectively when the first mouse in the experimental cohort (Hep3B-shACLY-Luc) reached endpoint. Liver and tumor tissues were weighed and collected for downstream analysis.

2.10.3 Bioluminescence Imaging

Tumor progression was monitored via bioluminescence imaging using IVIS Spectrum In Vivo Imaging System (Perkin Elmer Cat. No. 124262). Bioluminescence was achieved through intraperitoneal injection of D-Luciferin dissolved in saline (Sigma Aldrich Cat. No. S8776) at a concentration of 0.15 mg/g of bodyweight. IVIS imaging was performed on auto exposure setting at 10 minutes post-injection.

2.11 Data Mining and Statistical Analysis

Independent T-test, ANOVA were performed using GraphPad Prism 8 software. Spearman's correlation and regression analysis was performed using R studio. Statistical significance was defined as $p\text{-value} < 0.05$. Publicly available transcriptome datasets were obtained from NCBI Gene Expression Omnibus repository and The Cancer Genome Atlas (TCGA) database. Survival analysis was sourced from Kaplan-Meier Plotter.

CHAPTER III – RESULTS

Chapter III – Results:

3.1 Elevated expression of ACLY is characteristic of human HCC

To investigate if ACLY expression is altered in human hepatocellular carcinoma (HCC), we analyzed several publicly available patient derived transcriptome datasets with associated clinical annotations. Paired comparison between 247 patient tumor and adjacent non-tumor liver tissues revealed a significant increase in ACLY transcript abundance in tumors.[57](Figure 1A) Considering the progressive nature of liver disease leading up to HCC, we increased the resolution of analysis by comparing ACLY expression between stages of disease progression. Sourcing from the Wurmbach microarray dataset, we found that ACLY expression positively correlated with disease progression of HCV induced HCC.[58] (Figure 1B) Similarly, analysis of the Ye microarray dataset revealed differential expression of ACLY between primary and metastatic lesions among patients with HBV induced HCC.[59] (Figure 1C) Advanced and metastatic diseases lead to unfavorable survival outcome. As such, we stratified 364 HCC patients in TCGA Liver Hepatocellular Carcinoma database according to ACLY expression and examined their survival durations. Regardless of etiology, patients belonging to the lower tertile expression group displayed significantly longer survival compared to patients belonging to the higher tertile group.[60] (Figure 1D) Interestingly, this effect is most prominent among patients who were not diagnosed with hepatitis infection. Thus, ACLY expression correlates with disease progression and the poor clinical outcome among HCC patients.

3.2 DOX inducible shRNA construct temporally reduces ACLY expression in HCC

To validate the role of ACLY in HCC, we aimed to genetically ablate ACLY expression through inducible shRNA knockdown in HCC cell lines. The human Hep3B and SK-Hep1 cell lines were chosen due to their respective epithelial and mesenchymal phenotype which enables us to determine if the effects of ACLY inhibition are cell-line dependent.[61,62] Inducible knockdown of ACLY using 1 µg/mL DOX significantly reduced ACLY and p-ACLY S455 expression in both cell lines over the course of 7 days. (Figure 2A, 2B) Notably, short hairpin ACLY (shACLY) construct #1 reduced ACLY expression by greater than 95% in Hep3B cells.

Interestingly, ACLY knockdown in vitro did not affect the expression of genes that are involved in its metabolic and signalling network. (Figure 2C) Specifically, the expression of ACSS2 was not increased in contrast to previous studies reporting compensatory utilization of acetate upon ACLY inhibition.[52] Similarly, FASN and ACC, which act downstream of ACLY, are also unchanged, suggesting that de novo lipogenesis (DNL) may not be affected on a gene expression level. Previously, studies have implicated ACLY in tumor stemness and epithelial-mesenchymal transition.[40,41,47] However, ACLY deficiency in Hep3B cells neither altered the expression of epithelial marker E-cadherin nor the expression and phosphorylation of AKT which acts upstream of various oncogenic pathways controlling the aforementioned processes. Collectively, these results indicate that ACLY genetic ablation may have minimal effects on gene expression and warrant investigation of functional outcomes of ACLY deficiency.

3.3 ACLY deficiency reprograms DNL and sterol synthesis

Given the role of ACLY in lipid metabolism, we sought to determine if ACLY deficiency could alter DNL. Using [^{14}C] glucose, we identified a significant reduction in glucose mediated DNL in both Hep3B and SK-Hep1 cell lines. (Figure 3A, 3C) Similar to the differential potency between shACLY construct #1 and #2 with respect to ACLY knockdown, we also observed differential potency between the two constructs with respect to DNL, suggesting that reduction in glucose mediated DNL is ACLY specific. Interestingly, despite similar levels of ACLY expression between Hep3B and SK-Hep1-shACLY #1, glucose mediated DNL was completely abolished in SK-Hep1 cells while retaining approximately 60% activity in Hep3B cells.

Subsequently, we used [^{3}H] acetate to determine if reduction in glucose mediated DNL could lead to compensatory utilization of acetate. We found that [^{3}H] acetate mediated DNL is consistently upregulated in both SK-Hep1 and Hep3B cells. (Figure 3B, 3D) Additionally, acetate incorporation into lipids is negatively correlated with glucose mediated DNL upon ACLY knockdown. (Figure 3E) SK-Hep1-shACLY cells displayed higher levels of acetate incorporation compared to Hep3B-shACLY cells, corresponding to greater reduction in glucose mediated DNL. Similarly, shACLY construct #1 also induced higher levels of acetate incorporation compared to shACLY construct #2, further demonstrating that the observed compensatory mechanism is ACLY specific.

To determine if the observed compensatory utilization of acetate is mediated by ACSS2, we treated ACLY deficient cells with an ACSS2 chemical inhibitor (ACSS2i). Indeed, ACLY deficient Hep3B cells were significantly more sensitive to the inhibitory

effect of ACSS2i at 5 μM, demonstrating > 80% reduction of [3H] acetate mediated DNL compared to approximately 50% in control cells, suggesting that the compensatory mechanism is mediated by ACSS2 through increased substrate flux. (Figure 3F)

Acetyl-CoA is the substrate for both DNL and sterol synthesis, as such we aimed to elucidate if sterol synthesis would respond to ACLY knockdown similarly. However, contrary to our hypothesis, [^{14}C] glucose incorporation into sterol was not significantly altered while [^{3}H] acetate flux was upregulated. (Figure 4A, 4B) This effect was consistent between SK-Hep1 and Hep3B cells.

3.4 ACLY deficiency induces fatty acid oxidation

Reprogramming of lipid metabolism led us to investigate if lipid catabolism is also affected. Using [^{14}C] palmitic acid, we identified significantly elevated CO_2 release as a result of fatty acid oxidation. (Figure 5A, 5B) Likewise, acid soluble intermediates were also enriched. This effect was consistent between SK-Hep1 and Hep3B cell lines and is inversely proportional to the extent of ACLY knockdown.

Elevated levels of fatty acid oxidation led us to hypothesize if ACLY deficiency may lead to a more oxidative and less glycolytic phenotype. As such, we quantified the rate of extracellular lactate release as a measure of glycolysis in Hep3B cells. (Figure 5C) There was no significant difference in lactate release across time points of 4, 6 and 12 hours between control and ACLY deficient cells, suggesting that anerobic glucose utilization is not affected.

3.5 ACLY deficiency reduces cell proliferation, clonogenicity and migration in a cell-line dependent manner

We hypothesized that inhibition of ACLY could alter lipid metabolism leading to reduced cell proliferation. This was validated in SK-Hep1 cells which showed an approximately 30% reduction in cell proliferation over the course of 2 days. (Figure 6A) In contrast, this effect was absent in Hep3B cells which exhibit minimal alterations in cell proliferation and viability, suggesting a cell-line dependent phenomenon. (Figure 3A) However, ACLY deficiency significantly reduced the clonogenicity of Hep3B cells over the course of 7 days, suggesting that the ability for Hep3B cells to undergo cell autonomous mitosis is impaired. (Figure 6B) SK-Hep1 cells are not able to form colonies due to their mesenchymal morphology and high motility, however they are highly metastatic.[61] As such, we explored their migratory potential in vitro using the matrigel invasion assay which showed significant reductions in cell migration overnight upon ACLY knockdown. (Figure 6C)

3.6 In vivo knockdown of ACLY reduces hepatic tumor burden in NRG mice

To determine if ACLY deficiency leads to reduced tumor growth in vivo, we engineered DOX inducible Hep3B-shACLY and non-targeting shRNA (Hep3B-shNTC) cells expressing luciferase (Hep3B-shACLY/shNTC-Luc) and injected 1×10^6 cells into the livers of male NRG mice. After 7 days, we conducted bioluminescence imaging and grouped mice based on baseline bioluminescence intensity. We then induced ACLY knockdown with 2 μg/mL DOX in drinking water, ad libitum, and monitored tumor

progression for 6 weeks. (Figure 7A) Immunoblot analysis of protein expression confirmed knockdown of ACLY in vivo. (Figure 7B) However, residual ACLY expression remains in the tumor tissue potentially originating from other cell types or from growth selective pressure. Interestingly, ACSS2 was upregulated in ACLY deficient tumor in contrast to our previous observation in vitro. Bioluminescence intensity at end point and fold change compared to week 1 were not significantly different between +/- DOX cohorts for both Hep3B-shACLY-Luc and -shNTC-Luc mice. (Figure 7C) Similarly, the number of intrahepatic metastasis nodules are consistent between +/-DOX treated Hep3B-shACLY-Luc mice. (Figure 7D) However, resected liver tumor tissues from DOX induced Hep3B-shACLY-Luc cohort weighed significantly less compared to those from uninduced mice of the same cohort. (Figure 7E) The discrepancy between bioluminescence intensity and tumor weight may be attributed to extrahepatic lesions or luminescence detection sensitivity.

CHAPTER IV – FIGURES

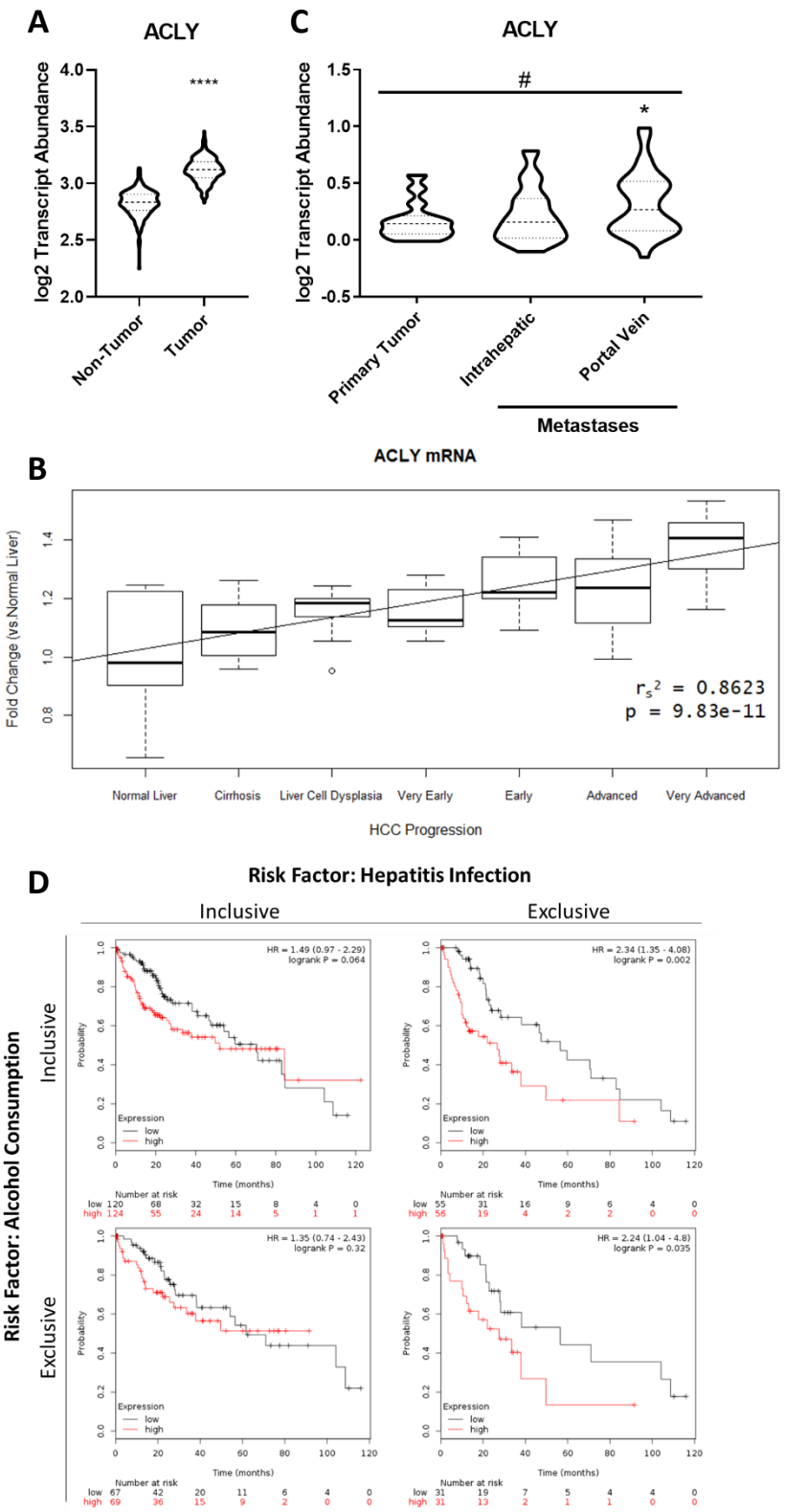
A
ACLY
log2 Transcript Abundance
4.0
3.5
3.0
2.5
2.0
****
Non-Tumor
Tumor
C
ACLY
log2 Transcript Abundance
1.5
1.0
0.5
0.0
-0.5
#
*
Primary Tumor
Intrahepatic
Portal Vein
Metastases
B
ACLY mRNA
Fold Change (vs Normal Liver)
0.8
1.0
1.2
1.4
r_s^2 = 0.8623
p = 9.83e-11
Normal Liver
Cirrhosis
Liver Cell Dysplasia
Very Early
Early
Advanced
Very Advanced
HCC Progression
D
Risk Factor: Hepatitis Infection
Inclusive
Exclusive
Risk Factor: Alcohol Consumption
Inclusive
Exclusive
HR = 1.49 (0.97 - 2.29)
logrank P = 0.064
HR = 2.34 (1.35 - 4.08)
logrank P = 0.002
HR = 1.35 (0.74 - 2.43)
logrank P = 0.32
HR = 2.24 (1.04 - 4.8)
logrank P = 0.035
Probability
Expression
low
high
Time (months)
Number at risk
low 120 68 32 15 8 4 0
high 124 55 24 14 5 1 1
low 55 31 16 9 6 4 0
high 56 19 4 2 2 0 0
low 67 42 20 11 6 4 0
high 69 36 15 9 2 0 0
low 31 19 7 5 4 4 0
high 31 13 2 1 1 0 0

Figure 1 – ACLY expression positively correlates with HCC progression. A) ACLY transcript abundance is upregulated in tumor compared to adjacent non-tumor liver samples. (**** denotes p-value <0.0001) B) ACLY expression positively correlates with liver disease progression. C) ACLY transcript abundance is significantly different between metastatic lesions and primary tumor. (# denotes one-way ANOVA p-value <0.05, * denotes Tukey's post-hoc comparison p-value <0.05) D) ACLY expression predicts poor patient survival according to HCC risk factors.

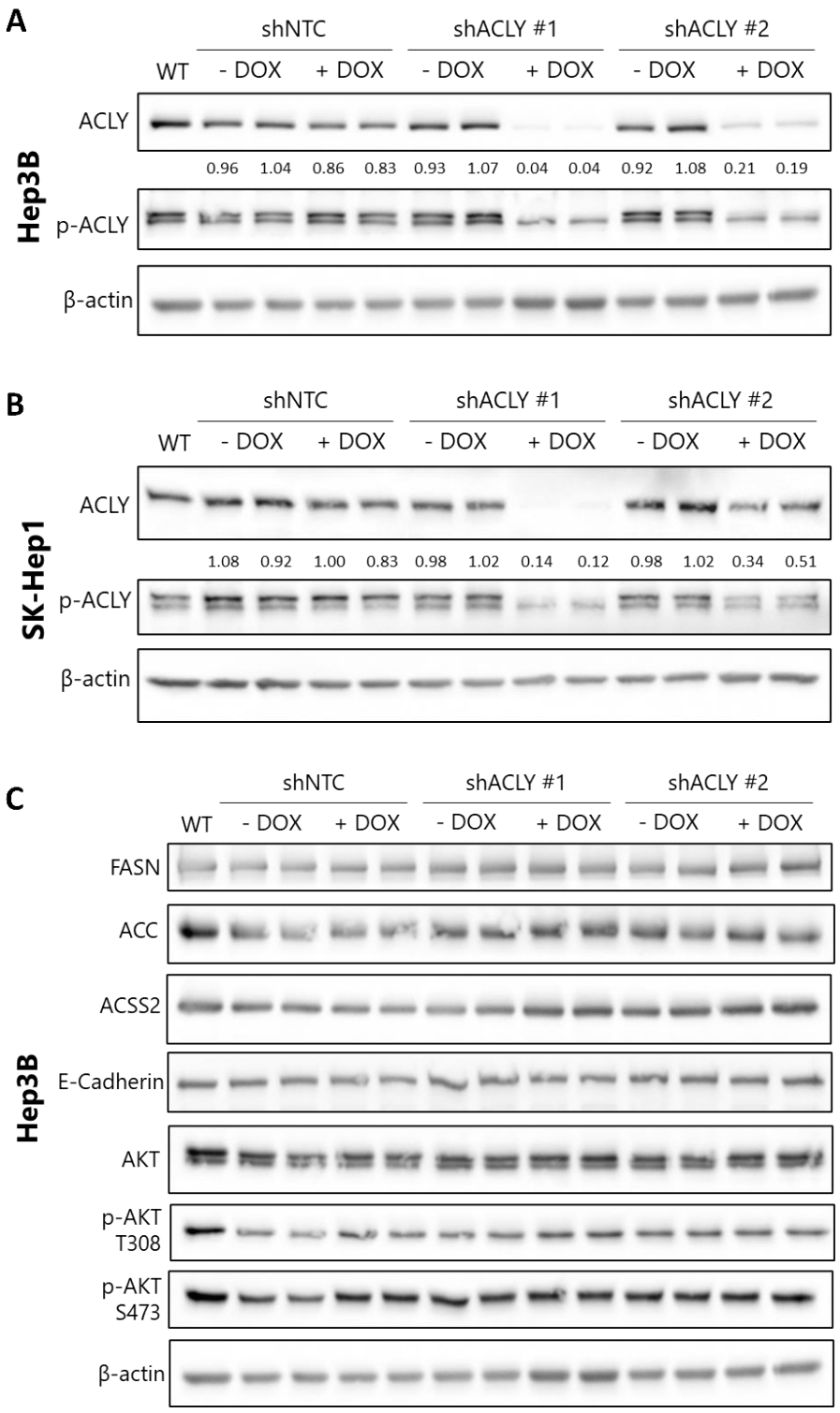
A
shNTC
shACLY #1
shACLY #2
WT
- DOX
+ DOX
- DOX
+ DOX
- DOX
+ DOX
Hep3B
ACLY
0.96 1.04 0.86 0.83 0.93 1.07 0.04 0.04 0.92 1.08 0.21 0.19
p-ACLY
β-actin
B
shNTC
shACLY #1
shACLY #2
WT
- DOX
+ DOX
- DOX
+ DOX
- DOX
+ DOX
SK-Hep1
ACLY
1.08 0.92 1.00 0.83 0.98 1.02 0.14 0.12 0.98 1.02 0.34 0.51
p-ACLY
β-actin
C
shNTC
shACLY #1
shACLY #2
WT
- DOX
+ DOX
- DOX
+ DOX
- DOX
+ DOX
Hep3B
FASN
ACC
ACSS2
E-Cadherin
AKT
p-AKT T308
p-AKT S473
β-actin

Figure 2 – Effects of inducible ACLY knockdown on protein expression. DOX inducible shRNA suppresses ACLY expression in A) Hep3B and B) SK-Hep1 cells. Densitometry quantification of protein abundance is expressed relative to β-actin. C) Analysis FASN, ACC, ACSS2, E-Cadherin, AKT/p-T308/p-S473 expression.

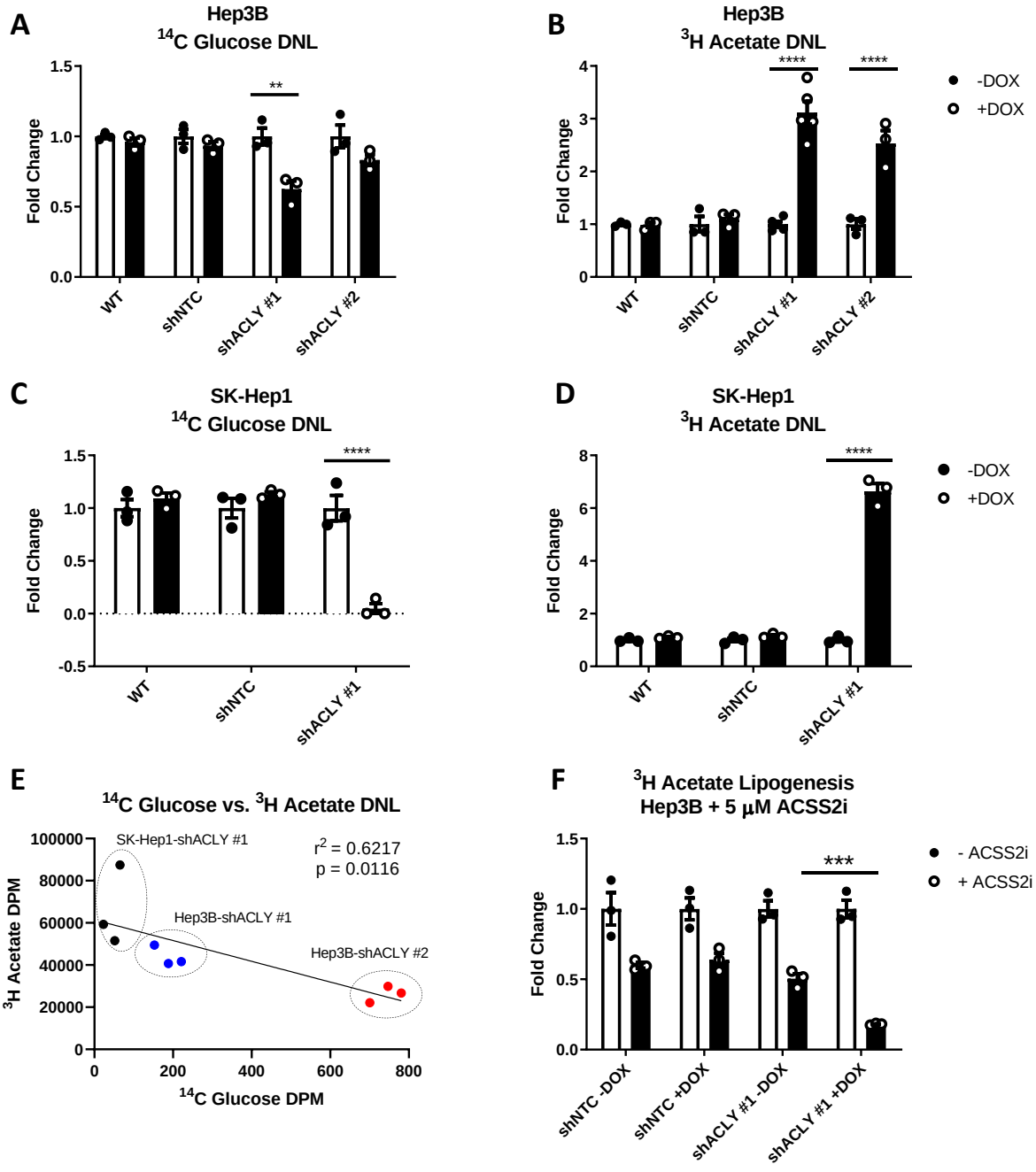
A
Hep3B
14C Glucose DNL
Fold Change
1.5
1.0
0.5
0.0
**
WT
shNTC
shACLY #1
shACLY #2
B
Hep3B
3H Acetate DNL
Fold Change
4
3
2
1
0
****
****
-DOX
+DOX
C
SK-Hep1
14C Glucose DNL
Fold Change
1.5
1.0
0.5
0.0
-0.5
****
WT
shNTC
shACLY #1
D
SK-Hep1
3H Acetate DNL
Fold Change
8
6
4
2
0
****
-DOX
+DOX
E
14C Glucose vs. 3H Acetate DNL
3H Acetate DPM
100000
80000
60000
40000
20000
0
0
200
400
600
800
14C Glucose DPM
SK-Hep1-shACLY #1
Hep3B-shACLY #1
Hep3B-shACLY #2
r2 = 0.6217
p = 0.0116
F
3H Acetate Lipogenesis
Hep3B + 5 µM ACSS2i
Fold Change
1.5
1.0
0.5
0.0
***
shNTC -DOX
shNTC +DOX
shACLY #1 -DOX
shACLY #1 +DOX
- ACSS2i
+ ACSS2i

Figure 3 – ACLY knockdown reprograms DNL. A – D) ACLY knockdown reduces [^{14}C] glucose mediated DNL while increasing [^{3}H] acetate mediated DNL in Hep3B and SK-Hep1 cells. (** denotes p-value < 0.01, **** denotes p-value < 0.0001). E) [^{14}C] glucose DNL is negatively correlated with [^{3}H] acetate DNL. F) ACLY deficient Hep3B cells are more sensitive to ACSS2i inhibition with respect to [^{3}H] acetate DNL. (*** denotes p-value < 0.001)

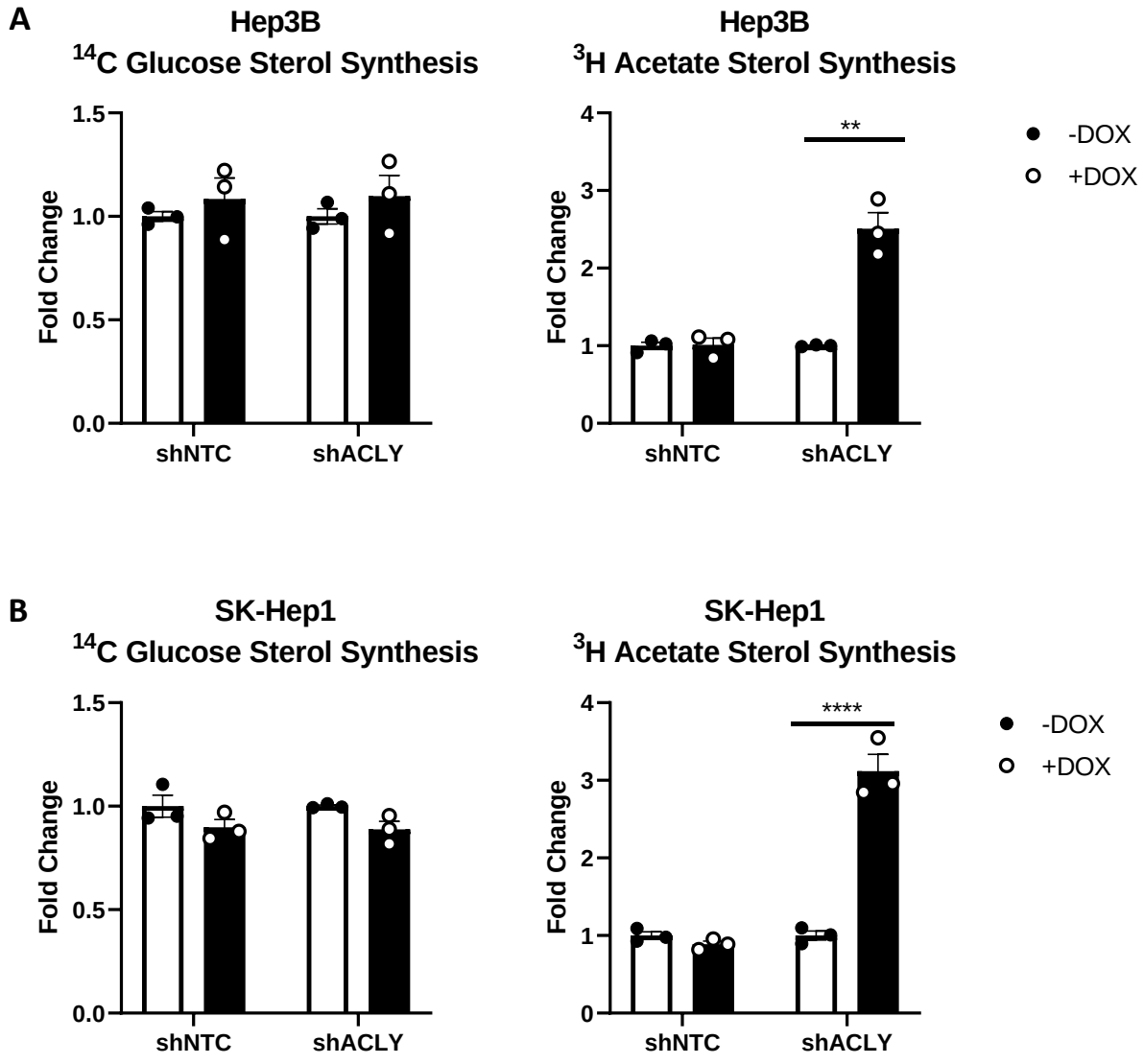

Figure 4 – ACLY knockdown induces sterol synthesis. ACLY knockdown increases [^{3}H] acetate sterol synthesis but does not affect [^{14}C] glucose sterol synthesis in A) Hep3B and B) SK-Hep1 cells. (** denotes p-value < 0.01, **** denotes p-value < 0.0001)

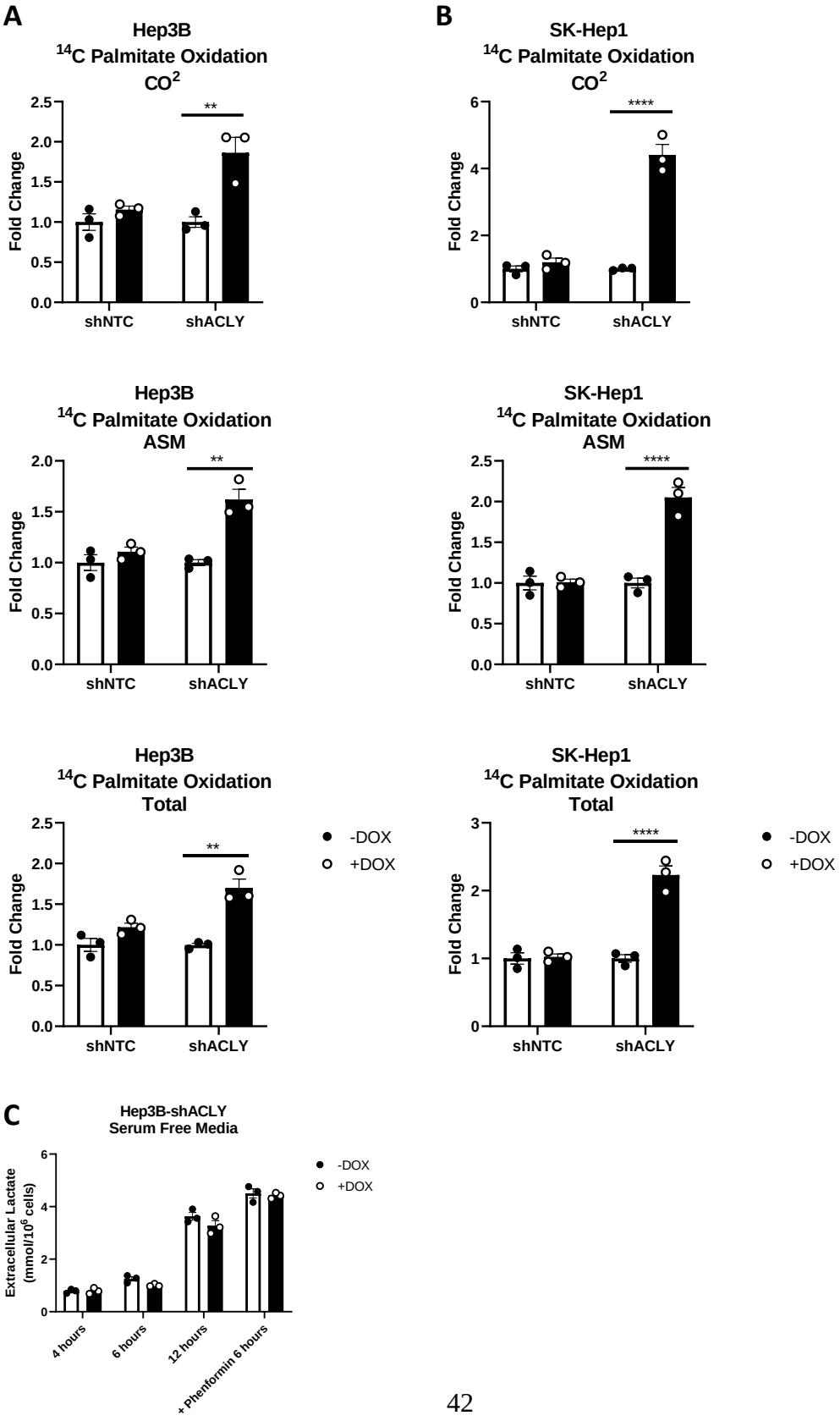
A
Hep3B
14C Palmitate Oxidation
CO2
Fold Change
shNTC
shACLY
B
SK-Hep1
14C Palmitate Oxidation
CO2
Hep3B
14C Palmitate Oxidation
ASM
SK-Hep1
14C Palmitate Oxidation
ASM
Hep3B
14C Palmitate Oxidation
Total
SK-Hep1
14C Palmitate Oxidation
Total
-DOX
+DOX
C
Hep3B-shACLY
Serum Free Media
Extracellular Lactate
(mmol/10^6 cells)
4 hours
6 hours
12 hours
+ Phenformin 6 hours

Figure 5 – ACLY knockdown induces fatty acid oxidation. ACLY knockdown increases fatty acid oxidation in A) Hep3B and B) SK-Hep1 cells. (** denotes p-value < 0.01, **** denotes p-value < 0.0001) C) ACLY knockdown does not affect extracellular lactate release in Hep3B cells.

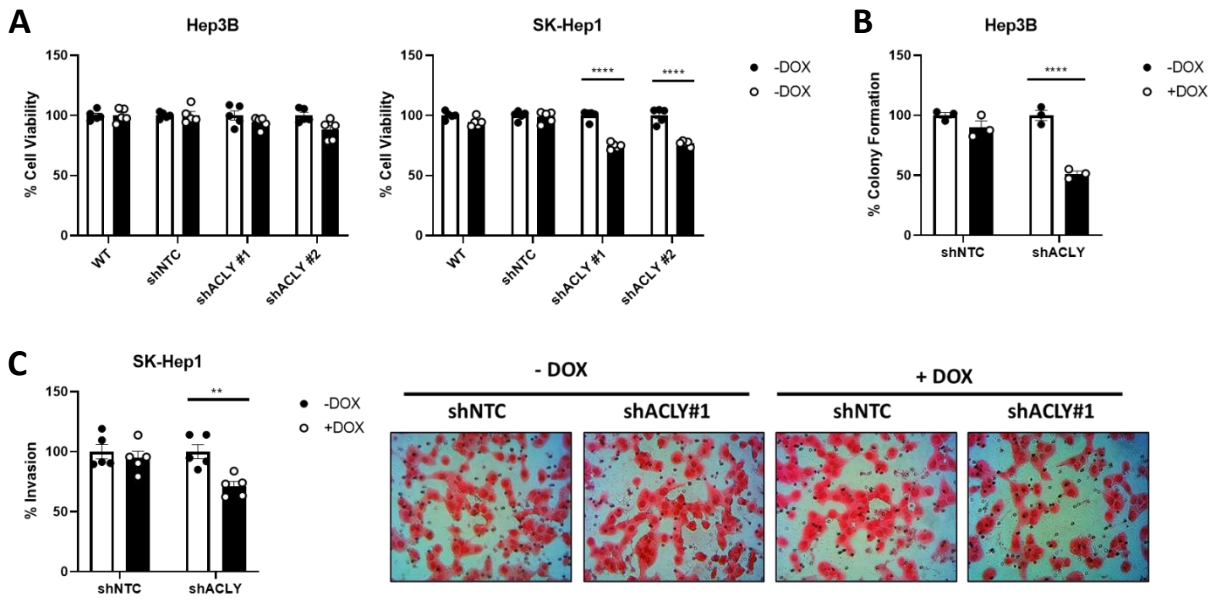

Figure 6 – ACLY knockdown reduces cell proliferation, clonogenicity and migration in a cell-line dependent manner. A) Hep3B and SK-Hep1 cells display differential response to ACLY deficiency with respect to cell proliferation. (**** denotes p-value < 0.0001) B) ACLY knockdown reduces Hep3B clonogenicity. (**** denotes p-value < 0.0001) C) ACLY knockdown reduces SK-Hep invasion across matrigel membrane. (** denotes p-value <0.01)

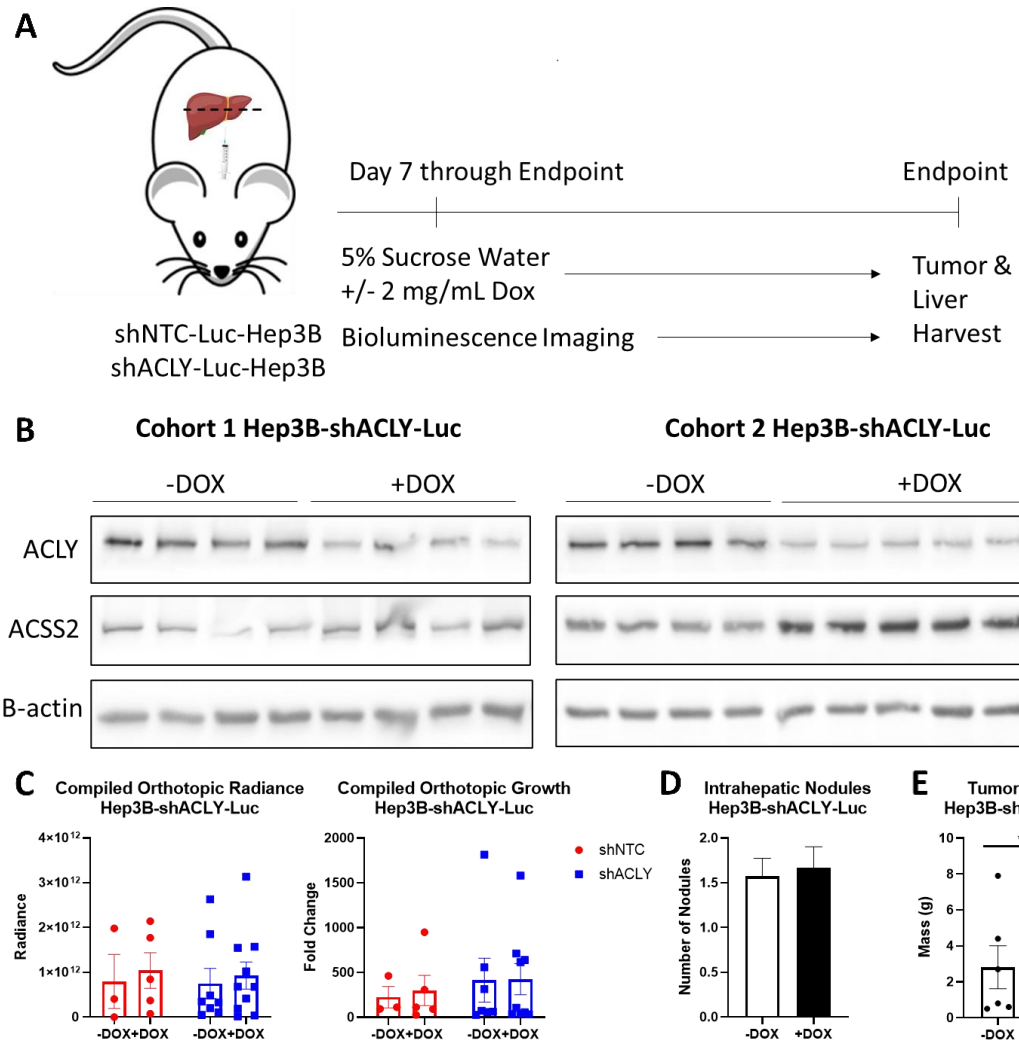
A
Day 7 through Endpoint
Endpoint
5% Sucrose Water
+/- 2 mg/mL Dox
Tumor &
Liver
Harvest
shNTC-Luc-Hep3B
shACLY-Luc-Hep3B
Bioluminescence Imaging
B
Cohort 1 Hep3B-shACLY-Luc
Cohort 2 Hep3B-shACLY-Luc
-DOX
+DOX
-DOX
+DOX
ACLY
ACSS2
B-actin
C
Compiled Orthotopic Radiance
Hep3B-shACLY-Luc
Radiance
4×10^12
3×10^12
2×10^12
1×10^12
0
-DOX+DOX
-DOX+DOX
Compiled Orthotopic Growth
Hep3B-shACLY-Luc
Fold Change
2000
1500
1000
500
0
-DOX+DOX
-DOX+DOX
shNTC
shACLY
D
Intrahepatic Nodules
Hep3B-shACLY-Luc
Number of Nodules
2.0
1.5
1.0
0.5
0.0
-DOX
+DOX
E
Tumor Weight
Hep3B-shACLY-Luc
Mass (g)
10
8
6
4
2
0
*
-DOX
+DOX

Figure 7 – In vivo ACLY knockdown in orthotopic tumor graft reduces tumor burden. A) Outline of in vivo experiment. B) ACLY expression is suppressed in vivo with concomitant upregulation of ACSS2 expression. C) Bioluminescence at 6 weeks is not different between control and ACLY deficient tumor. D) Livers injected with Hep3B-shACLY-Luc cells display similar numbers of intrahepatic nodules between +/- DOX cohorts. E) ACLY deficient tumors display reduced tumor weight. (* denotes p-value < 0.05)

CHAPTER V – DISCUSSION

Chapter V – Discussion

HCC is a multivariate disease with few distinguishing molecular features. Our investigation of the role ACLY plays in HCC thus began with the transcriptome analysis of patient derived HCC biopsies. We initially identified upregulation of ACLY expression in tumor biopsies belonging to HCC diseases of HBV and HCV etiology, two of the most prominent types of HCC.[57,59] However, considering that HCC is a progressive disease, we aimed to explore if this phenomenon correlated with progressive stages of HCC. Our analysis identified a positive, linear trend with respect to ACLY expression and HCC progression in the context of both primary HCC as well as metastatic disease.[58,59] This led us to hypothesize that ACLY expression may be relevant for advanced HCC and by extension, patient survival. As such, we stratified a population of HCC patients with mixed etiology into tertiles based on their ACLY expression and analyzed their survival distribution across 10 years.[60] Our initial analysis revealed a statistically insignificant difference in survival between patients belonging to the top and bottom tertile of ACLY expression. However, upon excluding patients with chronic hepatitis infection, the survival difference becomes significantly more pronounced. Hepatitis infection leads to HCC via genomic instability and development of cirrhosis.[63] These mechanisms are not dependent on deregulated lipid metabolism of which ACLY overexpression contributes to. In contrast, HCC that is induced by non-alcoholic fatty liver disease and alcohol consumption are dependent on deregulated lipid metabolism. As such, we have identified that elevated

ACLY expression is significantly associated with increased rate of patient mortality in HCC cases uncomplicated by hepatitis infection.

Previous research suggest that sensitivity to ACLY inhibition may be dependent on the preferential usage of glucose in cancer cells and that ACLY inhibition may induce tumor differentiation.[40,47,49] Hep3B cells have been shown to preferentially uptake glucose as opposed to acetate while SK-Hep1 cells display mesenchymal stem-like characteristics.[64,65] As such, we chose these two cells for modelling ACLY genetic inhibition. We employed a DOX inducible shRNA system to achieve temporal control over ACLY knockdown. Using this system, treatment with DOX mimics pharmacological targeting of ACLY. We designed and cloned 2 shACLY sequences targeting different loci of the ACLY transcript along with a non-targeting shRNA sequence as a negative control. Optimization of this system in vitro achieved stable and maximal knockdown 7 days after DOX induction at 1 μg/mL with no adverse effects on cell viability. However, shACLY #1 achieved substantially higher level of ACLY knockdown compared to shACLY #2 in both Hep3B and SK-Hep1 cell lines. This allowed us to validate the target specificity of ACLY knockdown in a gene dosage dependent manner when characterizing cell phenotype in response to ACLY knockdown.

We hypothesized that the expression of key components of acetyl-CoA and DNL pathways should respond in a compensatory manner upon ACLY knockdown. However, we found that ACC, FASN and ACSS2 expression were unchanged. These enzymes are responsible for the downstream catalysis of acetyl-CoA and the alternative synthesis of acetyl-CoA using acetate. The lack of response on a protein expression level suggests that

cell culture media conditions may circumvent the need for DNL in vitro or that elevated substrate flux may be compensatory instead. We also hypothesized that ACLY deficiency may lead to the inhibition of AKT activation and increase the expression of E-cadherin as observed in lung cancer cells.[41] This would support the notion that ACLY inhibition could lead to tumor differentiation which was observed in breast and lung cancer cells.[40] However, our immunoblot analysis did not detect significant change in the expression or phosphorylation of AKT or E-cadherin. This suggests that the previously observed effect on tumor differentiation and AKT signaling may be organ specific.

Although we detected significant ACLY knockdown in our immunoblot analysis, it was unknown if this would result in any alterations in phenotype. As such, we aimed to determine the functional outcome of ACLY deficiency through exploration of cell proliferation, clonogenicity and invasion. ACLY knockdown reduced the proliferation of SK-Hep1 cells but not that of Hep3B cells. However, the clonogenicity of Hep3B cells was significantly suppressed. This may highlight a paracrine signalling mechanism that enables Hep3B cells to survive ACLY deficiency in a cell proliferation experimental context. In contrast, due to low cell density in a colony formation experiment, paracrine signalling maybe lacking leading to an impairment of cell autonomous proliferation.

While SK-Hep1 cells are unable to form colonies due to their mesenchymal phenotype, we sought to explore the effect of ACLY deficiency on their invasive capacity. We found that the capacity for SK-Hep1 cells to migrate through a matrigel membrane were impaired. SK-Hep1 cells are metastatic in vivo. As such, it may be of interest to

elucidate the effect of ACLY knockdown on SK-Hep1 cells' metastatic potential through intrasplenic or tail vein injection in an immune-compromised animal model.

ACLY performs an important role in lipid metabolism by synthesizing acetyl-CoA from mitochondrial citrate. Therefore, we furthered our phenotype exploration of ACLY knockdown by examining its effect on DNL. We utilized radiolabelled [^{14}C] glucose to determine the incorporation of glucose into lipid and sterol fractions. The metabolism of glucose through glycolysis and the citric acid cycle produces citrate inside the mitochondria which is then exported into the cytosol for ACLY catalysis. ACLY knockdown significantly reduced the incorporation of glucose into lipid fractions in both Hep3B and SK-Hep1 cells. Furthermore, the proportions of inhibition corresponded with the proportions of ACLY knockdown that were differentially achieved by shACLY #1 and #2, suggesting that the observed phenomenon is a direct result of ACLY deficiency. Interestingly, while SK-Hep1 cells displayed nearly complete abolition of glucose mediated DNL, Hep3B cells retained approximately 50 – 60% of this activity. This illustrates a difference between SK-Hep1 and Hep3B cells with regards to their lipid metabolism. While SK-Hep1 cells seem to solely rely on ACLY to catalyze glucose mediated DNL, there may exist alternative pathways capable of converting glucose to lipid independent of ACLY in Hep3B cells. Indeed, Liu et al. recently demonstrated that mammalian cells are capable of synthesizing acetate de novo from glucose derived pyruvate, providing one potential explanation for our observation.[66]

To confirm the compensatory role of acetate under conditions of ACLY deficiency, we used [^{3}H] acetate to determine the proportion of its incorporation into lipid. We found

that acetate mediated DNL was significantly elevated in both Hep3B and SK-Hep1 ACLY deficient cells. Furthermore, regression analysis showed a significant negative correlation between glucose and acetate mediated DNL, suggesting that ACLY knockdown is causal of this phenomenon. Though our immunoblot analysis did not show increased expression of ACSS2, the enzyme responsible for converting acetate to acetyl-CoA, our observation here suggests that compensatory upregulation of the acetate DNL pathway may be mediated by increased substrate flux. We confirmed this by treating ACLY deficient cells with a chemical inhibitor targeting ACSS2 and found that ACLY deficient cells were significantly more sensitive to its inhibitory effect on acetate mediated DNL.

In line with our DNL observations, we hypothesized that cholesterol synthesis should respond similarly to ACLY deficiency due to the role of acetyl-CoA in the mevalonate pathway. However, we did not observe inhibition of glucose mediated sterol synthesis though acetate incorporation was elevated. This result suggests that glucose may not be the preferential source of carbon for sterol synthesis. Furthermore, acetate mediated sterol synthesis may be induced by ACLY deficiency due to the abundance of substrate availability.

Next, we explored the effect of ACLY deficiency on lipid catabolism. We used CO_2 as the surrogate reporter for fatty acid oxidation and isolated acid soluble intermediates to determine downstream citric acid cycle activity. Our result shows consistent increase in both measurements, suggesting that ACLY deficient cells increase the usage of lipid as an energy source. Previous research showed that malonyl-CoA, synthesized from acetyl-CoA by ACC, inhibits the translocation of fatty acids into mitochondria by CPT1.[43] As such,

ACLY deficiency may limit malonyl-CoA availability leading to the induction of fatty acid oxidation. The Warburg hypothesis postulates that cancer cells preferentially utilize anaerobic glycolysis for ATP production. Previous research suggests that fatty acid oxidation is induced to escape anoikis caused by loss of extracellular matrix attachment and the resultant inhibition of glucose uptake and glycolysis.[21] As such, the observed increase in fatty acid oxidation induced by ACLY deficiency led us to hypothesize if ACLY deficient cells may be less glycolytic. We quantified the concentration of lactate released extracellularly over 2, 4 and 6 hours, however there were no appreciable differences between ACLY deficient and non-deficient cells. Lactate is the product of pyruvate reduction and anerobic glycolysis. The lack of change in lactate release over the time course indicate that the increase in fatty acid oxidation is not a compensatory mechanism for impaired glycolysis.

Our in vitro characterization of cellular response to ACLY deficiency led us to explore if tumor growth is affected in vivo. We employed an immune-compromised orthotopic HCC model whereby equal numbers of Hep3B cells expressing luciferase and shRNA constructs were injected into the left lobe of the liver. Compared to xenograft models, orthotopic HCC growth is more biologically representative, in part due to the diverse metabolic microenvironment that is unique to the liver. We induced ACLY knockdown in vivo using 2 mg/mL DOX dissolved in 5% drinking water, a sufficiently potent concentration and stable solution validated by other studies.[67,68] Immunoblot analysis of isolated tumors demonstrated significant knockdown of ACLY expression, albeit not to the same extent as observed in vitro. This may be attributed to the presence of

non-Hep3B cells, such as endothelial cells and hepatocytes, that have infiltrated into the tumor. Secondly, selective growth pressure may have led to the clonal expansion of non-ACLY deficient Hep3B cells. We also identified ACSS2 upregulation in ACLY deficient tumor tissues, suggesting that compensatory activation of ACSS2 pathway may also occur in vivo. With respect to tumor growth, we observed inconsistent findings between measured tumor weights and bioluminescence. Specifically, quantification of total radiance did not show a difference between ACLY deficient and non-deficient cells at end point. However, tumor weights were significantly lower in the ACLY deficient cohort at the time of sacrifice. Furthermore, we observed intrahepatic metastases in both ACLY deficient and control cohorts. However, there was no significant difference in the number of intrahepatic nodules between the cohorts. The inconsistent finding between tumor weight and bioluminescence may be due to signal saturation using the IVIS imaging system. Furthermore, we occasionally observed large week-to-week variability in bioluminescence signal belonging to the same mice which diminishes the reliability of this surrogate measure.

Moving forward, several unanswered questions may be worth exploring in continuation of this study. Firstly, it is unknown if total DNL is altered in ACLY deficient tumor cells. We observed compensatory increase in acetate mediated DNL, however it is unclear if this exceeds basal DNL level in wildtype cells. The fates of glucose and acetate in DNL and cholesterol synthesis could be further elucidated with higher resolution through metabolic flux analysis. Specifically, it would be interesting to determine the contribution of glucose to the abundance of the various downstream substrates in the process of

cholesterol synthesis to pinpoint metabolites and chemical reactions that are affected by ACLY deficiency. In line with high-throughput analyses, we could also use RNA-Seq analysis to identify transcriptome profiles of ACLY deficient cells compared to that of control. Doing so, we could build on our targeted immunoblot analysis of select protein expression to identify alterations in molecular pathways that may be explanatory of our observed phenotypes. Furthermore, reprogramming of lipid metabolism may bring forth compensatory opportunistic molecular alterations that are suitable for dual inhibition along with ACLY. In our other experiments, we did not observe synergistic anti-proliferative effect of ACSS2 chemical inhibition in ACLY knockdown cells. However, a genome wide screen using CRISPR editing may reveal critical targets for cell metabolism yet unfound in our current study.

With respect to in vivo characterization of ACLY deficient tumors, we could perform histological analysis of tumor samples to compare disease stages and perform gene expression analysis to corroborate with RNA-Seq results. We could also improve the biological relevance of our study by developing a NASH driven HCC model via injection of tumor cells into mice with established NASH induced through feeding a diet high in fat and fructose. For this, we may employ a syngeneic mouse model with an intact immune system. Considering that NASH drastically alters the metabolic and immune microenvironments present in the liver, it would be interesting to study the interplay between tumor and immune cells along with the growth of ACLY deficient tumors in such conditions.

CHAPTER VI – CONCLUSION

Chapter VI – Conclusion

This study characterizes the role of ACLY in HCC. We began with correlational analysis of publicly available human HCC transcriptome datasets and identified a positive link between ACLY expression and tumor progression. We then engineered DOX inducible ACLY knockdown in Hep3B and SK-Hep1 cells to characterize alterations in protein expression, lipid metabolism and cell proliferation. This revealed the reprogramming of DNL, cholesterol synthesis and fatty acid oxidation in ACLY deficient cells along with inhibition of cell proliferation, clonogenicity and invasion in a cell dependent manner. Lastly, we performed in vivo characterization of ACLY deficient tumor growth whereby tumor cells were orthotopically injected in NRG mice. We validated in vivo ACLY knockdown and observed reduced tumor weight at end point. Collectively, these data indicate that pharmacologically targeting ACLY may elicit beneficial effects for treating HCC.

References:

1. Ferenci, P. *et al.* Hepatocellular Carcinoma (HCC). *J. Clin. Gastroenterol.* **44**, 239–245 (2010).
2. *Canadian Cancer Statistics*. https://www.cancer.ca/~/media/cancer.ca/CW/cancer information/cancer 101/Canadian cancer statistics/Canadian-Cancer-Statistics-2019-EN.pdf?la=en (2019).
3. Raza, A. & Sood, G. K. Hepatocellular carcinoma review: Current treatment, and evidence-based medicine. *World J. Gastroenterol.* **20**, 4115 (2014).
4. Tsim, N. C., Frampton, A. E., Habib, N. A. & Jiao, L. R. Surgical treatment for liver cancer. *World J. Gastroenterol.* **16**, 927–33 (2010).
5. El-Serag, H. B. Hepatocellular Carcinoma. *N. Engl. J. Med.* **365**, 1118–1127 (2011).
6. Llovet, J. M. *et al.* Sorafenib in Advanced Hepatocellular Carcinoma. *N. Engl. J. Med.* **359**, 378–390 (2008).
7. Kudo, M. *et al.* Lenvatinib versus sorafenib in first-line treatment of patients with unresectable hepatocellular carcinoma: a randomised phase 3 non-inferiority trial. *Lancet (London, England)* **391**, 1163–1173 (2018).
8. Sanyal, A. J., Yoon, S. K. & Lencioni, R. The etiology of hepatocellular carcinoma and consequences for treatment. *Oncologist* **15 Suppl 4**, 14–22 (2010).
9. Turati, F. *et al.* Metabolic syndrome and hepatocellular carcinoma risk. *Br. J. Cancer* **108**, 222–8 (2013).
10. Michelotti, G. A., Machado, M. V. & Diehl, A. M. NAFLD, NASH and liver

cancer. *Nat. Rev. Gastroenterol. Hepatol.* **10**, 656–665 (2013).

11. Schulze, K., Nault, J.-C. & Villanueva, A. Genetic profiling of hepatocellular carcinoma using next-generation sequencing. *J. Hepatol.* **65**, 1031–1042 (2016).
12. Bidkhori, G. *et al.* Metabolic network-based stratification of hepatocellular carcinoma reveals three distinct tumor subtypes. *Proc. Natl. Acad. Sci. U. S. A.* **115**, E11874–E11883 (2018).
13. Ookhtens, M., Kannan, R., Lyon, I. & Baker, N. Liver and adipose tissue contributions to newly formed fatty acids in an ascites tumor. *Am. J. Physiol. Integr. Comp. Physiol.* **247**, R146–R153 (1984).
14. Berndt, N. *et al.* Characterization of Lipid and Lipid Droplet Metabolism in Human HCC. *Cells* **8**, (2019).
15. MS, B. & JL, G. The SREBP Pathway: Regulation of Cholesterol Metabolism by Proteolysis of a Membrane-Bound Transcription Factor. *Cell* **89**, (1997).
16. Litwack, G. Human biochemistry. in (ed. Litwack, G.) 199–255 (2018).
17. Lally, J. S. V. *et al.* Inhibition of Acetyl-CoA Carboxylase by Phosphorylation or the Inhibitor ND-654 Suppresses Lipogenesis and Hepatocellular Carcinoma. *Cell Metab.* **29**, 174-182.e5 (2019).
18. Li, L. *et al.* Inactivation of fatty acid synthase impairs hepatocarcinogenesis driven by AKT in mice and humans. *J. Hepatol.* **64**, 333–341 (2016).
19. Ma, X.-L. *et al.* Sphere-forming culture enriches liver cancer stem cells and reveals Stearoyl-CoA desaturase 1 as a potential therapeutic target. *BMC Cancer* **19**, 760 (2019).

20. Ma, M. K. F. *et al.* Stearoyl-CoA desaturase regulates sorafenib resistance via modulation of ER stress-induced differentiation. *J. Hepatol.* **67**, 979–990 (2017).

21. Schafer, Z. T. *et al.* Antioxidant and oncogene rescue of metabolic defects caused by loss of matrix attachment. *Nature* **461**, 109–113 (2009).

22. Lu, G.-D. *et al.* CCAAT/enhancer binding protein α predicts poorer prognosis and prevents energy starvation-induced cell death in hepatocellular carcinoma. *Hepatology* **61**, 965–78 (2015).

23. Iwamoto, H. *et al.* Cancer Lipid Metabolism Confers Antiangiogenic Drug Resistance. *Cell Metab.* **28**, 104-117.e5 (2018).

24. Wang, M.-D. *et al.* Acetyl-coenzyme A carboxylase alpha promotion of glucose-mediated fatty acid synthesis enhances survival of hepatocellular carcinoma in mice and patients. *Hepatology* **63**, 1272–1286 (2016).

25. Huang, D. *et al.* HIF-1-mediated suppression of acyl-CoA dehydrogenases and fatty acid oxidation is critical for cancer progression. *Cell Rep.* **8**, 1930–1942 (2014).

26. Li, J. *et al.* CD147 reprograms fatty acid metabolism in hepatocellular carcinoma cells through Akt/mTOR/SREBP1c and P38/PPARα pathways. *J. Hepatol.* **63**, 1378–1389 (2015).

27. Fujiwara, N. *et al.* CPT2 downregulation adapts HCC to lipid-rich environment and promotes carcinogenesis via acylcarnitine accumulation in obesity. *Gut* **67**, 1493–1504 (2018).

28. Newman, T. B. & Hulley, S. B. Carcinogenicity of Lipid-Lowering Drugs. *JAMA*

J. Am. Med. Assoc. **275**, 55 (1996).

29. Vinogradova, Y., Coupland, C. & Hippisley-Cox, J. Exposure to statins and risk of common cancers: a series of nested case-control studies. *BMC Cancer* **11**, 409 (2011).

30. Jiang, S.-S. *et al.* The clinical significance of preoperative serum cholesterol and high-density lipoprotein-cholesterol levels in hepatocellular carcinoma. *J. Cancer* **7**, 626–32 (2016).

31. Yang, Z. *et al.* Cholesterol inhibits hepatocellular carcinoma invasion and metastasis by promoting CD44 localization in lipid rafts. *Cancer Lett.* **429**, 66–77 (2018).

32. Jiang, Y. *et al.* Proteomics identifies new therapeutic targets of early-stage hepatocellular carcinoma. *Nature* **567**, 257–261 (2019).

33. Liang, J. Q. *et al.* Dietary cholesterol promotes steatohepatitis related hepatocellular carcinoma through dysregulated metabolism and calcium signaling. *Nat. Commun.* **9**, 4490 (2018).

34. Klein, C. A. CANCER: The Metastasis Cascade. *Science (80-.).* **321**, 1785–1787 (2008).

35. Tolba, R., Kraus, T., Liedtke, C., Schwarz, M. & Weiskirchen, R. Diethylnitrosamine (DEN)-induced carcinogenic liver injury in mice. *Lab. Anim.* **49**, 59–69 (2015).

36. Migita, T. *et al.* Inhibition of ATP Citrate Lyase Induces an Anticancer Effect via Reactive Oxygen Species: AMPK as a Predictive Biomarker for Therapeutic

Impact. *Am. J. Pathol.* **182**, 1800–1810 (2013).

37. Yancy, H. F. *et al.* Metastatic progression and gene expression between breast cancer cell lines from African American and Caucasian women. *J. Carcinog.* **6**, 8 (2007).

38. Halliday, K. R., Fenoglio-Preiser, C. & Sillerud, L. O. Differentiation of human tumors from nonmalignant tissue by natural-abundance 13C NMR spectroscopy. *Magn. Reson. Med.* **7**, 384–411 (1988).

39. Pinkosky, S. L., Groot, P. H. E., Lalwani, N. D. & Steinberg, G. R. Targeting ATP-Citrate Lyase in Hyperlipidemia and Metabolic Disorders. *Trends Mol. Med.* **23**, 1047–1063 (2017).

40. Hatzivassiliou, G. *et al.* ATP citrate lyase inhibition can suppress tumor cell growth. *Cancer Cell* **8**, 311–321 (2005).

41. Hanai, J. *et al.* Inhibition of lung cancer growth: ATP citrate lyase knockdown and statin treatment leads to dual blockade of mitogen-activated protein kinase (MAPK) and phosphatidylinositol-3-kinase (PI3K)/AKT pathways. *J. Cell. Physiol.* **227**, 1709–20 (2012).

42. Okabayashi, T. *et al.* Glycolysis module activated by hypoxia-inducible factor 1α is related to the aggressive phenotype of hepatocellular carcinoma. *Int. J. Oncol.* **33**, 725–731 (1992).

43. Foster, D. W. Malonyl-CoA: the regulator of fatty acid synthesis and oxidation. *J. Clin. Invest.* **122**, 1958–9 (2012).

44. Ference, B. A. *et al.* Mendelian Randomization Study of *ACLY* and Cardiovascular

Disease. *N. Engl. J. Med.* **380**, 1033–1042 (2019).

45. Wang, Q. *et al.* Abrogation of hepatic ATP-citrate lyase protects against fatty liver and ameliorates hyperglycemia in leptin receptor-deficient mice. *Hepatology* **49**, 1166–1175 (2009).

46. Berwick, D. C., Hers, I., Heesom, K. J., Moule, S. K. & Tavare, J. M. The identification of ATP-citrate lyase as a protein kinase B (Akt) substrate in primary adipocytes. *J. Biol. Chem.* **277**, 33895–900 (2002).

47. Hanai, J., Doro, N., Seth, P. & Sukhatme, V. P. ATP citrate lyase knockdown impacts cancer stem cells in vitro. *Cell Death Dis.* **4**, e696–e696 (2013).

48. Singh, A. & Settleman, J. EMT, cancer stem cells and drug resistance: an emerging axis of evil in the war on cancer. *Oncogene* **29**, 4741–4751 (2010).

49. Migita, T. *et al.* ATP Citrate Lyase: Activation and Therapeutic Implications in Non-Small Cell Lung Cancer. *Cancer Res.* **68**, 8547–8554 (2008).

50. Zhou, Y. *et al.* ATP Citrate Lyase Mediates Resistance of Colorectal Cancer Cells to SN38. *Mol. Cancer Ther.* **12**, 2782–2791 (2013).

51. Migita, T. *et al.* Inhibition of ATP Citrate Lyase Induces an Anticancer Effect via Reactive Oxygen Species: AMPK as a Predictive Biomarker for Therapeutic Impact. *Am. J. Pathol.* **182**, 1800–1810 (2013).

52. Zhao, S. *et al.* ATP-Citrate Lyase Controls a Glucose-to-Acetate Metabolic Switch. *Cell Rep.* **17**, 1037–1052 (2016).

53. Comerford, S. A. *et al.* Acetate Dependence of Tumors. *Cell* **159**, 1591–1602 (2014).

54. Zhao, S. *et al.* Dietary fructose feeds hepatic lipogenesis via microbiota-derived acetate. *Nature* **579**, 586–591 (2020).

55. Jang, C. *et al.* The Small Intestine Converts Dietary Fructose into Glucose and Organic Acids. *Cell Metab.* **27**, 351 (2018).

56. Frank, S. B., Schulz, V. V & Miranti, C. K. A streamlined method for the design and cloning of shRNAs into an optimized Dox-inducible lentiviral vector. *BMC Biotechnol.* **17**, 24 (2017).

57. Roessler, S. *et al.* A Unique Metastasis Gene Signature Enables Prediction of Tumor Relapse in Early Stage Hepatocellular Carcinoma Patients. *Cancer Res.* **70**, 10202 (2010).

58. Wurmbach, E. *et al.* Genome-wide molecular profiles of HCV-induced dysplasia and hepatocellular carcinoma. *Hepatology* **45**, 938–947 (2007).

59. Ye, Q.-H. *et al.* Predicting hepatitis B virus–positive metastatic hepatocellular carcinomas using gene expression profiling and supervised machine learning. *Nat. Med.* **9**, 416–423 (2003).

60. Menyhárt, O., Nagy, Á. & Győrffy, B. Determining consistent prognostic biomarkers of overall survival and vascular invasion in hepatocellular carcinoma. *R. Soc. Open Sci.* **5**, 181006 (2018).

61. Fuchs, B. C. *et al.* Epithelial-to-Mesenchymal Transition and Integrin-Linked Kinase Mediate Sensitivity to Epidermal Growth Factor Receptor Inhibition in Human Hepatoma Cells. *Cancer Res.* **68**, 2391–2399 (2008).

62. Eun, J. R. *et al.* Hepatoma SK Hep-1 Cells Exhibit Characteristics of Oncogenic

Mesenchymal Stem Cells with Highly Metastatic Capacity. *PLoS One* **9**, e110744 (2014).

63. Villanueva, A. Hepatocellular Carcinoma. *N. Engl. J. Med.* **380**, 1450–1462 (2019).

64. Yun, M. *et al.* The importance of acetyl coenzyme A synthetase for 11C-acetate uptake and cell survival in hepatocellular carcinoma. *J. Nucl. Med.* **50**, 1222–8 (2009).

65. Hashimoto, N. *et al.* Cancer stem-like sphere cells induced from de-differentiated hepatocellular carcinoma-derived cell lines possess the resistance to anti-cancer drugs. *BMC Cancer* **14**, 722 (2014).

66. Liu, X. *et al.* Acetate Production from Glucose and Coupling to Mitochondrial Metabolism in Mammals. *Cell* **175**, 502-513.e13 (2018).

67. Redelsperger, I. M. *et al.* Stability of Doxycycline in Feed and Water and Minimal Effective Doses in Tetracycline-Inducible Systems. *J. Am. Assoc. Lab. Anim. Sci.* **55**, 467 (2016).

68. Ganguly, S. S. *et al.* Notch3 promotes prostate cancer-induced bone lesion development via MMP-3. *Oncogene* **39**, 204–218 (2020).